

The Great Observatories Origins Deep Survey: Constraints on the Lyman Continuum Escape Fraction Distribution of Lyman–Break Galaxies at $3.4 < z < 4.5$ ¹

E. VANZELLA², M. GIAVALISCO³, A. INOUE⁴, M. NONINO², F. FONTANOT², S. CRISTIANI², A. GRAZIAN⁵, M. DICKINSON⁶, D. STERN⁷, P. TOZZI², E. GIALLONGO⁵, H. FERGUSON⁸, H. SPINRAD⁹, K. BOUTSIA⁵, A. FONTANA⁵, P. ROSATI¹⁰

²*INAF – Trieste Astronomical Observatory, via G.B. Tiepolo 11, 40131 Trieste, Italy*

³*Department of Astronomy, University of Massachusetts, Amherst MA 01003, USA*

⁴*College of General Education, Osaka Sangyo University, 3-1-1, Nakagaito, Daito, Osaka 574-8530, Japan*

⁵*INAF - Rome Astronomical Observatory, Via Frascati 33, I-00040 Monteporzio Roma, Italy*

⁶*NOAO, PO Box 26732, Tucson, AZ 85726, USA*

⁷*Jet Propulsion Laboratory, California Institute of Technology, Mail Stop 169-527, Pasadena, CA 91109, USA*

⁸*STScI, 3700 San Martin Dr., Baltimore, MD 21218, USA*

⁹*Department of Astronomy, University of California, Berkeley, CA 94720, USA*

¹⁰*ESO, Karl Schwarzschild Strasse 2, 85748, Garching, Germany*

ABSTRACT

We use ultra-deep ultraviolet VLT/VIMOS intermediate-band and VLT/FORS1 narrow-band imaging in the GOODS Southern field to derive limits on the distribution of the escape fraction (f_{esc}) of ionizing radiation for $L \geq L_{z=3}^*$

¹Based on observations made at the European Southern Observatory Very Large Telescope, Paranal, Chile (ESO programme 170.A-0788 The Great Observatories Origins Deep Survey: ESO Public Observations of the SST Legacy / *HST* Treasury / *Chandra* Deep Field South). Also based on observations obtained with the NASA/ESA *Hubble Space Telescope* obtained at the Space Telescope Science Institute, which is operated by the Association of Universities for Research in Astronomy, Inc. (AURA) under NASA contract NAS 5-26555.

Lyman Break Galaxies (LBGs) at redshift 3.4–4.5. Only one LBG, at redshift $z = 3.795$, is detected in its Lyman continuum (LyC; $S/N \simeq 5.5$), the highest redshift galaxy currently known with a direct detection. Its ultraviolet morphology is quite compact ($R_{\text{eff}} = 0.8$ kpc physical). Three out of seven AGN are also detected in their LyC, including one at redshift $z = 3.951$ and $z_{850} = 26.1$. From stacked data (LBGs) we set an upper limit to the average f_{esc} in the range 5%–20%, depending on how the data are selected (e.g., by magnitude and/or redshift). We undertake extensive Monte Carlo simulations that take into account intergalactic attenuation, stellar population synthesis models, dust extinction and photometric noise in order to explore the moments of the distribution of the escaping radiation. Various distributions (exponential, log-normal and Gaussian) are explored. We find that the median f_{esc} is lower than $\simeq 6\%$ with an 84% percentile limit not larger than 20%. If this result remains valid for fainter LBGs down to current observational limits, then the LBG population might be not sufficient to account for the entire photoionization budget at the redshifts considered here, with the exact details dependent upon the assumed ionizing background and QSO contribution thereto. It is possible that f_{esc} depends on the UV luminosity of the galaxies, with fainter galaxies having higher f_{esc} , and estimates of f_{esc} from a sample of faint LBG from the HUDF ($i_{775} \leq 28.5$) are in broad quantitative agreement with such a scenario.

Subject headings: cosmology: observations — galaxies: formation — galaxies: evolution — galaxies: distances and redshifts

1. Introduction

The fraction of the metagalactic ionizing background contributed by star-forming galaxies remains poorly constrained by direct measures at every cosmic epoch because of the difficulty of the observations. In particular, we do not have direct empirical determinations of how the fraction of escaping ionizing radiation depends on the properties of the galaxies, nor how it evolves with redshift. Yet, the issue deserves attention, because it directly bears on fundamental problems of galaxy evolution, such as the evolution of the initial mass function (IMF) and the contribution of galaxies to cosmic re-ionization.

The latter problem is currently particularly timely since observations are starting to identify relatively large samples of galaxies at $z > 7$ (e.g., Bouwens et al. 2010a,b; Finkelstein et al. 2010; Castellano et al. 2010), namely during the epoch when cosmic re-ionization is believed to have completed (e.g., Fan et al. 2002). The ultraviolet background (UVB)

radiation can significantly affect galaxy evolution by photo-ionizing and heating the interstellar medium (ISM) to $\sim 10^4$ K thereby decreasing gas accretion onto low-mass galaxies and evaporating the existing gas in small haloes. Deriving empirical constraints to the nature and evolution of the cosmic UVB, as well as the nature of ionizing sources, remains a primary goal of many observations.

Faucher-Giguère et al. (2008a) analyzed the opacity of the Lyman alpha forest (LAF) of 86 high-resolution quasar (QSO) spectra and found that the hydrogen photoionization rate Γ is remarkably flat in the redshift range 2 – 4.2. The quasar contribution to the hydrogen ionizing background increases toward $z \sim 2$ as the peak of the quasar luminosity function is approached (e.g., Hopkins et al. 2007); beyond redshift 2 their contribution significantly decreases (e.g., Fontanot et al. 2007; Siana et al. 2008; Faucher-Giguère et al. 2009; Prochaska et al. (2009)). Glikman et al. (2010) calculate the faint-end slope of the QSO luminosity function and find that quasars might be able to ionize the intergalactic medium at $z \simeq 4$. However, recent additional observations improve their constraints on the slope, bringing it into greater agreement with previous estimates and suggesting that QSOs *may not* be sufficient to account for the ionizing photons (Glikman et al., in preparation). Star-forming galaxies are now known to exist numerously at these redshifts and are therefore the leading candidates to account for the remaining ionizing photons (e.g., Siana et al. 2008; Faucher-Giguère et al. 2009).

From the theoretical point of view, current predictions of the escape fraction of ionizing photons from high-redshift galaxies are confusing, with different results obtained by different simulations. For example, Gnedin et al. (2008) argued that f_{esc} , i.e., ratio of the flux density of Lyman continuum (LyC) escaping from a galaxy to that produced in the galaxy, increases with increasing halo mass in the range of $M_h = 10^{10} - 10^{12} M_\odot$, and their values of f_{esc} are mostly less than a few per cent. This is much lower than other published work; for example, Wise & Cen (2009) predict $f_{\text{esc}} \sim 0.4$. Yajima et al. (2010) found an opposite behavior such that f_{esc} decreases with increasing halo mass, with an average $f_{\text{esc}} = 0.40$ for $M_h = 10^9 M_\odot$ dropping to $f_{\text{esc}} = 0.07$ for $M_h = 10^{11} M_\odot$. A similar result was also found by Razoumov & Sommer-Larsen (2010). It is clear that the physical processes that modulate the escaping ionizing photons are not well understood.

From the observational point of view, f_{esc} has been poorly constrained due to the fact that LyC photons are easily absorbed by both the IGM and the interstellar medium in a galaxy. The best way to investigate the LyC emissivity from high-redshift galaxies is to perform deep spectroscopic or narrow-band observations focused on the peak of the LyC emission, e.g., 880–910Å rest-frame. Ultra-deep intermediate-band imaging can also give an important contribution, as we show in this work.

The LyC measure has been addressed in recent years by several authors. Malkan et al. (2003) and Siana et al. (2007, 2010) stacked tens of deep ultraviolet images of galaxies at $z \sim 1$ and report no detection. Similarly, Cowie et al. (2009) combined ~ 600 galaxies at $z \sim 1$ observed with *GALEX* and also report a nondetection. At higher redshift, Steidel et al. (2001) initially found $f_{\text{esc,rel}} \gtrsim 0.5$ from the composite spectrum of 29 Lyman Break Galaxies (LBGs) at $z \sim 3$, where $f_{\text{esc,rel}}$ is the *relative* fraction of escaping LyC (900 Å) photons relative to the fraction of escaping non-ionizing ultraviolet (1500 Å) photons. Giallongo et al. (2002) and Inoue et al. (2005) estimated an upper limit of $f_{\text{esc,rel}} \lesssim 0.1 - 0.4$ for a sample of LBGs at $z \sim 3$. Shapley et al. (2006; S06 hereafter) directly detected the escaping ionizing photons from two LBGs in the SSA22 field at $z = 3.1$, and estimated the average value of $f_{\text{esc,rel}} = 0.14$. Chen et al. (2007) placed a 95% confidence level upper limit of 0.075 for the escaping radiation at $z \geq 2$ of star-forming regions hosting gamma-ray bursts. More recently, Iwata et al. (2009) detected the LyC emission from 10 Ly- α emitters (LAEs) and 7 LBGs within a sample of 198 LAEs and LBGs in the SSA22 field. They showed that the mean value of $f_{\text{esc,rel}}$ for the 7 LBGs is 0.11 after correcting for dust extinction, and 0.20 if IGM absorption is taken into account.

Current observations suggest that f_{esc} increases with increasing redshift: the fraction of direct LyC detection grows from 0 to $\sim 10\%$ over the redshift range $0 < z < 3$ (e.g., Inoue et al. 2006). Even though the trend is possibly present, the current fraction of direct LyC detections may be overestimated due to contamination by blue light coming from lower redshift sources superimposed on the targeted LBG. This has been investigated in detail by Vanzella et al. (2010b), exploiting the high quality data of the Great Observatories Origins Deep Surveys (GOODS; Giavalisco et al. 2004a) and *Hubble* Ultra Deep Field projects (HUDF; Beckwith et al. 2006) in conjunction with ultra-deep VLT/VIMOS *U*-band imaging (Nonino et al. 2009). They find that the probability that at least $\sim 1/3$ of the direct detections reported in the literature are due to superposition of lower redshift sources (confused in the PSF of the image) is larger than 50%. Therefore the observed evolution of f_{esc} with redshift may be less pronounced than currently believed.

It is therefore necessary to perform LyC measurements as free as possible from contamination by lower redshift sources. An ideal starting point is therefore deep, high resolution, multi-wavelength (space-based) imaging. In the present work we address this issue exploiting the extensive information (spectroscopy and photometry) available in the GOODS Southern field and the HUDF. In particular, we take advantage of the deep VLT/FORS1 $7' \times 7'$ narrow-band 3880 Å imaging centered in the HUDF and ultra-deep intermediate-band VLT/VIMOS *U*-band imaging of the entire GOODS-South (Nonino et al. 2009).

Throughout this paper magnitudes are reported in the AB scale (Oke 1974), and the

world model, when needed, is a flat universe with density parameters $\Omega_m = 0.3$, $\Omega_\Lambda = 0.7$ and Hubble constant $H_0 = 73 \text{ km s}^{-1} \text{ Mpc}^{-1}$.

2. Data and sample selection

2.1. Intermediate-band (IB) imaging

Ultra-deep U intermediate-band imaging in the GOODS-South field was performed with the VLT/VIMOS imaging spectrograph for a total integration time of ~ 40 hours. Nonino et al. (2009) described the reduction and characterization of the final image quality, which reaches a depth of magnitude 29.5, 29.1 and 28.6 at 2σ , 3σ and 5σ within $1.2''$ aperture diameters, respectively (see Table 1). Completeness and detection limit analyses have been performed by running Monte Carlo simulations and we refer the reader to Nonino et al. (2009) for details. The seeing of the co-added image is $\simeq 0.8''$ and represents the deepest image currently available in the U band. The depth and the overall image quality of the co-added data, $\simeq 30 \text{ AB}$ at 1σ , are well matched to the impressive multiwavelength data available in GOODS-South.

The transmission of the filter is shown in Figure 1. The filter probes the LyC region ($\lambda < 912\text{\AA}$) for sources at redshift higher than 3.386. In the following we only consider sources with redshift higher than 3.4, for which the Lyman limit is beyond the red limit of the filter. The transmission at $\lambda > (912\text{\AA} \times 4.4)$ decreases rapidly to zero, and is never higher than 1% of its peak at $\simeq 3900\text{\AA}$. The filter has a FWHM of $\sim 350\text{\AA}$, corresponding to 80–60 \AA rest-frame for redshift 3.4–4.5, which makes it an intermediate-band filter (IB, hereafter). While the lower limit of the redshift range investigated in this work is set by the filter transmission, the upper limit is given by the gradual increase of opacity of the IGM. Indeed, as we discuss in detail in Sect. 4.1, the average transmission of the IGM decreases as redshift increases, reaching a transmission smaller than 3×10^{-4} (1.0 means 100% transmission) at redshift beyond 4.5. Therefore the transparency is too small at higher redshift to make analysis of $z > 4.5$ galaxies useful. In the following we adopt redshift 4.5 as an upper limit.

2.2. Narrow-band (NB) imaging

Very deep VLT/FORS1 narrow-band imaging (NB hereafter) has been performed in the GOODS-South field, including the HUDF, centered at $\alpha=3^h32^m32^s.88$, $\delta=-27^d47^m16^s$ (J2000) with a total exposure time of 60,900 seconds. These data were obtained with the goal of detecting Ly α emission at $z = 2.2$ (see Hayes et al. 2010 for details). The filter has

a central wavelength (λ_C) of 3880 Å, a width (FWHM) of $\Delta\lambda=37$ Å, and is sensitive to the LyC region for galaxies with redshift higher than 3.300. For the redshift range $3.3 < z < 4.5$, the NB filter probes rest-frame wavelengths $902 \text{ Å} > \lambda > 700 \text{ Å}$.

The data were reduced using standard tasks in NOAO/IRAF, including bias subtraction, flat field correction, and sky subtraction. Images were then registered onto a common astrometric grid and co-added. The resulting magnitude limit of ~ 26.5 at 5σ within a aperture diameter of $2''$ and the median seeing of the final image of $0.85''$ are fully consistent with the reduction of Hayes et al. (2010). In particular, the NB image reaches the magnitude limit of ~ 29.0 at 1σ within a $1.2''$ diameter aperture (see Table 1). The observed field is a sub-region of the larger IB imaging, and therefore the available LBG sample with spectroscopic redshifts is smaller ($\simeq 1/4$ of the full sample used in the VIMOS IB image). However, useful constraints can be derived from a stacking analysis (see Sect. 5). In the following we mainly exploit the deeper and wider IB imaging.

2.3. The spectroscopic sample

Extensive spectroscopic redshift surveys have been performed in the GOODS-South and surrounding fields (e.g., Cristiani et al. 2000; Szokoly et al. 2004; Vanzella et al. 2006, 2008; Popesso et al. 2008; Balestra et al. 2010; Stern et al., in preparation). A collection of the published surveys is available at the ESO web site¹. In the present work, only sources with secure redshifts are considered, i.e., those with the highest quality. All the spectra and the identified spectral features have been visually inspected.

The ESO/VIMOS spectroscopic survey extends beyond the deep GOODS-South area, where the IB photometry is also available. In this extended region we find 13 galaxies with secure redshifts in the range $3.4 < z < 4.5$.

In total, 135 sources in the IB image (122 in the GOODS-South area and 13 outside) have secure redshifts in the range $3.4 < z < 4.5$. Their redshift and i_{775} magnitude distributions are shown in Figure 2. The mean redshift and i_{775} magnitude of the sample are 3.64 ± 0.27 and 24.85 ± 0.58 , respectively.

¹<http://www.eso.org/sci/activities/projects/goods/>

3. The IB photometry and selection of the *clean* sample

Aperture photometry in the IB image was performed with SExtractor (Bertin & Arnouts 1996) in “double image” mode. To detect sources we have created a new, fake image based on the IB one with pixel values set to zero anywhere except at the positions of the LBGs satisfying our selection criteria, which were set to 10,000. Using these positions, photometry was then performed on the IB image. The accuracy in the centering of the apertures has been tested on a sample of 68 spectroscopically identified stars with magnitude z_{850} in the range 21 – 25 uniformly distributed across the IB image. The comparison between the original coordinates in the GOODS-South ACS catalog (v2.0) and those obtained by SExtractor on the corresponding “forced” positions in the IB image shows a mean deviation of $\langle \Delta_{\text{RA}} \rangle = 0.001 \pm 0.133''$ and $\langle \Delta_{\text{DEC}} \rangle = -0.009 \pm 0.136''$, which is significantly smaller than 1 pixel (0.3''). Flux measurements within increasing aperture diameters of 1.2'', 1.5'', 1.8'' and 2.1'' (4, 5, 6, 7 pixels) have been computed. The same procedures have been executed for the NB image.

Figure 3 shows the distribution of the IB signal-to-noise (S/N) ratios for the 135 galaxies in 1.2'' and 2.1'' apertures. The distributions are asymmetric, peaked around zero, and have a wider dispersion for the larger aperture. In the positive tails of the distributions there are possible direct LyC detections or intercepted foreground blue sources that mimic ionizing emission (we refer to the latter as *contaminants*, see next section). 35 out of 135 sources have a S/N ratio in the IB image higher than 2 in either the 1.2'' or 2.1'' aperture. All have been visually inspected in the IB and the *HST* images (see Figures 4, 5 and 6 and Appendix A for a description of the sample in the outer region of the GOODS-South area). The majority are due to offset faint or bright sources that boost the flux measure in the aperture centered on the LBG. In these cases the S/N ratio increases as the aperture diameter increases, because the contribution of the nearby source also increases. Relatedly, if the signal arises from the center of the aperture (i.e., at the LBG position), the S/N typically decreases as the aperture size increases. Illustrative examples of clear foreground contamination by bright, lower redshift galaxies include J033217.39-274142.4, J033212.98-274841.1, J033225.16-274852.6 and J033238.87-274908.7. Examples with a distinct and offset faint, blue source clearly visible in the ACS images that significantly (if not totally) contribute to the aperture photometry include J033204.87-274451.4, J033220.97-275022.3, J033226.49-274124.0 and J033236.83-274558.0; the last one is in the HUDF and was discussed in Vanzella et al. (2010b; see Figure 7). Since we generally do not have the redshift of these faint, blue compact sources, it is not possible to guarantee that they are in the foreground. However, we note that the number of faint, nearby sources is consistent with the expected superposition probability (see next section).

In the following, the $1.2''$ apertures are used to derive constraints on the escaping LyC radiation from LBGs. Moreover the two sigma limit has been adopted as the main IB detection threshold (results are also presented for 3 and 5 sigma limits). We identify 27 out of 135 sources that most probably suffer contamination by an offset foreground source in the $1.2''$ apertures. They are excluded in the following analysis. However, it is worth noting that we would tend to underestimate the derived constraints on f_{esc} if some of these offset sources are not foreground contamination.

We are most interested in investigating the contribution of stellar emission to the UVB. Therefore, AGNs are excluded from the sample as identified using either the 2 Ms *Chandra* image of GOODS-South (Luo et al. 2008) or by looking for typical AGN features like N V, Si IV and C IV emission lines in the spectra. We find that 7 out of the 135 sources are AGNs, one of which is contaminated by a nearby, foreground source (e.g., is one of the 27 sources mentioned above). The AGN image cutouts, photometric and spectroscopic information are reported in Figure 8. Ingoing the contaminated source, three out of the six remaining AGNs are detected in the IB image with a $S/N > 2$ (two with $S/N \sim 3$ and one with $S/N \sim 2$), i.e., at wavelengths bluer than 896\AA rest-frame. For the highest redshift source, GDS J033238.76-275121.6 at $z = 3.951$, the IB samples the rest-frame interval 700\AA - 808\AA .

In summary, among the 135 sources (122 in the GOODS-South area and 13 outside), 128 are LBGs and 7 are AGNs. Twenty-seven sources are contaminated (26 LBGs and one AGN); the distribution of IB flux densities of the uncontaminated sources is shown in Figure 9. Of the 102 isolated LBGs, 92 are from the GOODS-South area and 10 are from the surrounding region (see Figure 10). Images of the 26 contaminated LBGs (23 in the GOODS-South area and 3 in the outer region) are shown in Figures 6 and 11 (see Table 2 for a summary).

The sample of 102 *clean* LBGs is used to constrain the ionizing radiation escape fraction. In the following section we briefly discuss the expected likelihood of foreground superposition that can contaminate LyC measurements.

3.1. Foreground contamination

Vanzella et al. (2010b) discuss in detail the role of foreground contamination in estimating the LyC radiation from galaxies at redshift higher than 3. Taking advantage of the ultra-deep imaging available in the GOODS-South field, they show that the probability of a foreground source mimicking LyC emission is not negligible. For example, there is a 50% chance that at least 15% of a given sample is affected by superposition by lower redshift

sources for $1''$ seeing and a U -band magnitude limit of 28.5 (Vanzella et al. 2010b). Comparisons with the observations of Steidel et al. (2001) and Shapley et al. (2006) have been performed using Monte Carlo simulations. Taking this contamination effect into account (which increases with redshift), Vanzella et al. (2010b) estimates that the escape fraction might be overestimated (amplified) by up to a factor of two.

In this work we find contamination by both bright and faint sources (Figures 4 and 5). Considering the present spectroscopic sample of 135 sources, including the 7 AGNs, we find 27 sources (one AGN and 26 LBGs) are contaminated by lower redshift interlopers.

The probability that at least 13 high-redshift galaxies out of 135 are confused with a foreground object in a circle of $0.8''$ radius and U -band magnitude down to 29.5 is $\sim 50\%$ (adopting the U -band number counts reported in Nonino et al. 2009 and Vanzella et al. 2010b). However, the present analysis finds 27 contaminations out of a sample of 135. The apparent inconsistency with the above calculation is solved if the size of the nearby sources is taken into account. Indeed, we clearly note from ACS and IB images that many extended foreground galaxies still pollute the photometry of the background LBG at separations even larger than $1''$. Looking carefully at Figure 11 (and Figures 4 and 5) it is apparent that $\simeq 12$ out of 27 offset IB detections arise from relatively close, compact blue sources at separations of $\sim 1''$. This is fully consistent with the expected probability of a close superposition. The other superpositions are associated with tails of extended galaxies at larger separations.

If we relax the above calculation and adopt a circle of radius $1.2''$ to calculate the interloper rate, the probability that at least 27 galaxies out of 135 are polluted is $\sim 63\%$. A dedicated analysis should be performed to include the effect of size in these calculations, but that is beyond the scope of the present work. The main aim here is to select a sample as *clean* as possible and provide constraints on the escaping ionizing radiation.

3.2. The LyC detections

Four sources have been detected in their LyC (see Table 3). Three out of four are AGNs, two of them are in the Szokoly et al. (2004; S04) spectroscopic catalog and one has been observed in Cristiani et al. (2000; C00) and Balestra et al. (2010). The remaining source is an LBG observed with the Keck-DEIMOS spectrograph (Stern et al., in preparation). Summarizing the LyC detections,

1. J033204.94-274431.7 : AGN. C IV and N V emission lines are detected. No X-ray signal is measured in the 2Ms *Chandra* observations.

2. J033216.64-274253.3 : LBG. Ly α , Si IV and C IV (faint) absorption lines are detected.
3. J033238.76-275121.6 : AGN. C IV, C III], C II and X-ray emission are detected.
4. J033244.31-275251.3 : AGN. Ly α , N V, Si IV and X-ray emission are detected.

3.2.1. LyC emission from the LBG GDS J033216.64-274253.3

Among the 102 LBGs in the *clean* sample, only one is detected in the IB image (GDS J033216.64-274253.3 at $z = 3.795$; detected with $S/N \simeq 5.5$). The GOODS ACS images show that the source is quite compact, yet well resolved (SExtractor stellarity index of 0.43 in the z_{850} band) with effective radius $R_{\text{eff}} = 0.8$ kpc physical ($R_{\text{eff}} = 0.114''$), and has blue rest-frame ultraviolet continuum ($i_{775} - z_{850}$) = -0.015 ($\beta = -2.1$). There are no close sources in the ACS images that might affect the IB signal. Since it is isolated and compact, the probability that another compact foreground source is superposed along the line of sight within a circle of radius R_{eff} is lower than 0.1%. This is the highest redshift LBG currently known with direct LyC detection. The Keck-DEIMOS spectrum (Figure 12) shows a clear Ly α break with a mean continuum decrement $D_A = 0.61 \pm 0.03$, consistent with the expected IGM transmission at redshift 3.8 (e.g., Inoue & Iwata 2008). The spectrum also shows faint Si IV and C IV absorption lines. Interestingly, the low and high ionization absorption lines are weak (or absent), in contrast to typical LBG spectra where weak interstellar absorption lines are often associated with strong Ly α emission, and, conversely, Ly α in absorption is often accompanied with strong interstellar absorption lines (e.g., Shapley et al. 2003; Vanzella et al. 2009; Balestra et al. 2010). This source appears to be the fortuitous combination of a relatively high escape fraction of ionizing radiation with low IGM attenuation. From the multi-wavelength information (MUSIC catalog, Grazian et al. 2006; Santini et al. 2009) we derive the following best-fit parameters for this galaxy using the libraries of Bruzual & Charlot (2003) and a Salpeter IMF (similar values are obtained using the libraries of Charlot & Bruzual 2007): extinction $A_{1500} \sim 0.62$ (assuming a Calzetti et al. (2000) extinction law), age $\lesssim 0.1$ Gyr, star formation rate $\text{SFR} \sim 26 M_{\odot} \text{yr}^{-1}$ and stellar mass $M_{\star} \sim 2.7 \times 10^9 M_{\odot}$. On the one hand, if we assume an IGM transmission of 100%, a lower limit of 15% is obtained for f_{esc} . On the other hand, an f_{esc} of 100% corresponds to an IGM transmission not lower than 0.15. We note that in this extreme case, no Ly α in emission is expected as all of the ionizing radiation escapes. Moreover, the lower limit on the transmission of 0.15 is higher than the expected average value at this redshift, 0.022, and the probability to have a transmission higher than 0.15 at $z=3.8$ varies between 4.5% and 8% (see simulations in Sect. 4). This indicates a line of sight particularly free from Lyman limit systems.

3.2.2. LyC emission from AGNs and their influence on the IB photometry

It is worth noting that the three AGNs with LyC detections are not likely to be altering the transmission of the IGM in their spatial proximity, including the volume probed by our U -band images. Following D’Odorico et al. (2008; see also Cen & Haiman 2000), we calculated the radius of the sphere of influence (or Strömngren sphere) of each of the detected AGN by relating the intensity of the ultraviolet ionizing background at the Lyman limit to the luminosity of the source at the same frequency. The resulting radius is smaller than 750 kpc (physical) for all three AGNs. In particular, the faintest and highest redshift of them, J033238.76-275121.6 at $z = 3.951$, is detected at $S/N=3.3$ in the IB image (i.e., ~ 28.5) at a rest-frame wavelength blueward of 808\AA . Its influence on the surrounding IGM reaches a radius of only $\simeq 250$ kpc (physical). Indeed, the flux in the U -band would be completely suppressed if a Lyman limit system was intercepted in the redshift range $3.386 - 3.951$ (i.e., in the wavelength interval between the red edge of the U filter and the Lyman limit of the source). Since the Strömngren sphere radius is only 250 kpc (physical), the AGN is not influencing the IB observation, or in other words, the source must ionize the IGM at least down to redshift 3.386 to perturb the IB photometry ($\Delta z \geq 0.56$), which clearly is not the case. Its LyC detection is therefore most probably due to an intrinsically high transmission of the IGM and/or escape fraction of ionizing radiation.

Similarly, if f_{esc} is intrinsically high for the LBGs considered here as well, we expect a certain number of detections in the ultra-deep IB image (see below). In other words, the LyC detection of some of the AGNs validates the statistical method adopted here in constraining the f_{esc} distribution for galaxies.

The next section describes Monte Carlo simulations performed with the aim of constraining the f_{esc} distribution. A deeper limit on its average is given in Sect. 5 by stacking the sources.

4. Constraining the distribution of escaping ionizing radiation

In the following analysis we refer to the *clean* spectroscopic sample described in the previous sections, composed by 102 galaxies with one LyC detection at $S/N \simeq 5.5$. Once this *clean* spectroscopic sample of LBGs has been identified, it is interesting to address the following question: how many sources do we expect to detect at a given depth in the IB survey assuming a distribution function of f_{esc} ?

Allowing redshift to vary from 3.3 to 4.5, the IB filter probes rest-frame wavelengths far below 912\AA (e.g., down to $\sim 700\text{\AA}$), where the IGM transmission decreases rapidly to

zero because of the increasing probability of intercepting Lyman limit systems and damped Ly α systems (hereafter LLSs and DLAs, respectively) as well as the decreasing free path of ionizing photons (see next section). It is therefore necessary to estimate the expected LyC signal in our IB image adopting a model of the IGM transmission. This is also useful for the source stacking (Sect. 5).

4.1. Modeling the IGM transmission

The effective optical depth through a clumpy IGM at the rest-frame frequency ν_S for a source at redshift z_S is (e.g., Paresce, McKee & Bowyer 1980):

$$\tau_{\text{eff}}(\nu_S, z_S) = \int_0^{z_S} dz \int_{N_1}^{N_u} dN_{\text{HI}} \frac{\partial^2 \mathcal{N}}{\partial z \partial N_{\text{HI}}} (1 - e^{-\tau_{\text{cl}}}), \quad (1)$$

where $\partial^2 \mathcal{N} / \partial z \partial N_{\text{HI}}$ is the number of absorbers along the line of sight per unit redshift z interval and per unit HI column density N_{HI} interval, and $\tau_{\text{cl}} = \sigma_{\text{HI}}(\nu_S(1+z)/(1+z_S))N_{\text{HI}}$ is the optical depth of an absorber with N_{HI} at z , where $\sigma_{\text{HI}}(\nu)$ is the HI cross section at frequency ν in the absorber's rest-frame.² If the column density distribution of the absorbers is a power-law with index $-\beta$ ($\beta \approx 1.5$; e.g., Kim et al. 2002) independent of redshift, the maximum contribution to τ_{eff} is made by absorbers with $\tau_{\text{cl}} \sim 1$. Therefore, the absorption of the Lyman continuum is mainly caused by LLSs and DLAs with $N_{\text{HI}} > 10^{17} \text{ cm}^{-2}$ and not by the LAF, which has $N_{\text{HI}} \sim 10^{13} \text{ cm}^{-2}$. This implies that LyC absorption is very stochastic because it is related to the probability of intercepting a LLS.

In this work the intergalactic absorption derived from the Monte Carlo simulations of Inoue & Iwata (2008) is adopted (IW08 hereafter). Briefly, we recall the main steps. The simulations are based on an empirical distribution function of intergalactic absorbers which reproduces the observational statistics of the LAF, LLSs and DLAs simultaneously. From this assumed distribution function, a large number of absorbers have been generated (running suitable Monte Carlo simulations) along many lines of sight. The probability to encounter an absorber is assumed to follow a Poisson distribution, and for each one the column density and Doppler parameter are extracted randomly from their (empirical) probability distribution functions. Typically $\sim 18,000$ absorbers are generated for a line of sight in the redshift interval $0 < z < 6$ (this number depends on the lower limit to the column density). As described in detail in IW08, 10,000 lines of sight have been calculated in the redshift interval

²The frequency dependence of $\sigma_{\text{HI}}(\nu)$ for LyC is approximately $\propto \nu^{-3}$.

$3.4 \leq z \leq 4.5$ with step $\Delta z=0.1$. The resulting mean intergalactic transmission is comparable to that derived by Meiksin (2006) in the Lyman series regime ($\lambda > 912\text{\AA}$), though the IW08 transmission are slightly lower in the LyC regime. This is due to the different number of LLSs considered by the two approaches (see IW08 for details).

Figure 13 shows examples of transmissions along different line of sights, extracted randomly from the 10,000 realizations at the three redshifts $z = 3.4, 3.7$ and 4.0 . In some cases the transmission drops to zero blueward of the redshift of LLSs; in others the signal coming from the source is transmitted down to $\simeq 700\text{\AA}$. In general, as redshift increases, the IB filter used here is strongly penalized. This is shown in Figure 14, where the medians and 68% confidence interval of the transmissions of 10,000 different lines of sight calculated in the redshift range 3.4–4.5 are reported (the averages are also shown as open squares). The distributions are not symmetric because of intervening LLSs and DLAs. The transmissions have been convolved with the IB filter shape; therefore, they are calculated in the suitable wavelength interval covered by the filter at a given redshift. For comparison, the median transmissions calculated in the wavelength range 880-910 \AA is also shown (it is identical to that reported in Figure 8 of IW08). Clearly the transmissions calculated through the IB filter are systematically lower than the “optimal” case (880-910 \AA). This is fully taken into account in the simulations we describe in the following section. We note that at redshifts beyond 4.0, the intergalactic absorption strongly attenuates the ionizing flux.

We briefly note the recent findings of Prochaska et al. (2010), in which they find a significantly lower incidence of LLSs at $z < 4$ compared with previous estimates. A similar result have been found by Songaila & Cowie (2010), even though this tendency is less pronounced. Qualitatively, if these results are correct then the transmission of the IGM derived here is underestimated; i.e., the number of expected LyC detections in our IB survey would increase, and given the observational constraint of only one out of 102 LBGs detected, this would imply that the upper limits we derive for f_{esc} are further strengthened (see next section). Indeed, the fact that we detect two sources in their LyC (one LBG and one AGN) at relatively high redshift ($z \sim 4$) may support a higher average transmission than predicted from our simulations.

Quantitatively, the detailed inclusion of the results of Prochaska et al. (2010) (and Prochaska et al. 2009; Songaila & Cowie 2010) in the modeling of the IGM (as in IW08) deserves a dedicated work that will be presented elsewhere (Inoue et al. 2010). However, a comparison between the observations of Péroux et al. (2005; e.g., those adopted in IW08), Prochaska et al. (2010) and Songaila & Cowie (2010), shows that decreasing the mean LyC optical depth (due to a lower number density of LLSs) increases the final IGM transmission by a factor of 1.5 (see Figure 15).

In Sect. 5 we report limits on f_{esc} by stacking and considering previous and current statistics on LLSs.

4.2. Simulating the expected number of LyC detections

The *relative* fraction of escaping LyC photons (at 900 Å) relative to the fraction of escaping non-ionizing ultraviolet (1500 Å) photons is defined as (Steidel et al. 2001):

$$f_{\text{esc,rel}} \equiv \frac{(L1500/L900)_{\text{int}}}{(F1500/F900)_{\text{obs}}} \exp(\tau_{900}^{\text{IGM}}), \quad (2)$$

where $(F1500/F900)_{\text{obs}}$, $(L1500/L900)_{\text{int}}$ and τ_{900}^{IGM} represent the observed 1500 Å/900 Å flux density ratio, the intrinsic 1500 Å/900 Å luminosity density ratio, and the line-of-sight opacity of the IGM for 900 Å photons, respectively. Equation (2) compares the observed flux density ratio (corrected for the IGM opacity) with models of the ultraviolet spectral energy distribution of star-forming galaxies. If the dust attenuation A_{1500} is known, $f_{\text{esc,rel}}$ can be converted to f_{esc} as $f_{\text{esc}} = 10^{-0.4A_{1500}} f_{\text{esc,rel}}$ (e.g., Inoue et al. 2005; Siana et al. 2007). We can rearrange the above equation to give an estimation of the observed flux at wavelengths smaller than the Lyman limit (i.e., F_{LyC} instead of $F900_{\text{obs}}$):

$$F_{\text{LyC}} = \left(\frac{L\lambda_{\text{rest}}}{L1500} \right)_{\text{int}} f_{\text{esc}} \times (F1500)_{\text{obs}} \times e^{-\tau_{\lambda}^{\text{IGM}}} \times 10^{0.4 \times A_{1500}}, \quad (3)$$

The quantities on the right side of the equation have been modeled and inserted in a Monte Carlo simulation. They are described as follows:

1. $\left(\frac{L1500}{L\lambda_{\text{rest}}} \right)_{\text{int}}$: Depending on the redshift, the wavelength range probed by the IB filter is included in the interval $\lambda_{\text{rest}} < 908 \text{Å}$ ($=\lambda_{\text{rest}}(\text{max})=4000 \text{Å}/(1+z_{\text{min}})$ with $z_{\text{min}}=3.405$). The value of the intrinsic luminosity density ratio $(L1500/L\lambda_{\text{rest}})_{\text{int}}$ is still very uncertain observationally; it must therefore be estimated from stellar population synthesis models. The LyC flux is emitted by O stars, whose lifetime is much shorter than the B and A stars that dominate the 1500 Å flux emission. Therefore the luminosity ratio depends on the stellar population age, metallicity, star formation history (single burst, exponential decay, constant or multi-bursts) and IMF (e.g., Bruzual & Charlot 2003; Leitherer et al. 1999). When the dying O stars are not replenished with new star formation, the ratio increases rapidly within a few million years (e.g., single burst). In the case of constant star formation rate (SFR), O stars are continuously formed

and the A and B stars accumulate, so the ratio slowly increases and saturates at later times, beyond 1 Gyr (Siana et al. 2007). Inoue et al. (2005), adopting the Starburst 99 models (Leitherer et al. 1999) and assuming a constant SFR, Salpeter IMF over the mass range $0.1\text{-}100M_{\odot}$ and a metallicity Z of $0.001\text{-}0.02$ (0.02 is the Solar value), obtained ratios that lie in the $1.5 < (L1500/L900)_{\text{int}} < 5.5$ interval. Depending on the time since the onset of star formation, they reported $(L1500/L700)_{\text{int}} = 4.0$ (7.0) in the case of 10 Myr (100 Myr) old stellar populations, with the value saturating at older ages. Here, wavelengths below 900\AA are observed (down to $\simeq 750\text{\AA}$) with the IB filter passing from redshift 3.4 to 4.5 and therefore a suitable ratio must be considered. Adopting an average age of $\simeq 300$ Myr for our sample (derived by Pentericci et al. 2007, 2010), and following the calculations of Siana et al. (2007) that reported ratios between 6 and 8 for $(L1500/L900)_{\text{int}}$ and $(L1500/L700)_{\text{int}}$ for a similar age, respectively, and Inoue et al. (2005) that reported a ratio $\simeq 7$, we adopt a value of $(L1500/L_{\text{LyC}})_{\text{int}} \simeq 7$ for the following analysis. This has been used in the Monte Carlo simulations described below, where we assume a Gaussian distribution with a mean of 7 and a standard deviation 50% of the mean. The 50% scatter includes the dispersion due to different physical properties of the LBGs in the sample as well as their redshift distribution. Results do not change significantly if we allow it to vary between 30% and 70%.

2. **(F1500)_{obs}**: The $(F1500)_{\text{obs}}$ is derived from the observed i_{775} magnitude of each source. That filter corresponds to $\lambda_{\text{eff}} \sim 1750\text{\AA}$, 1550\AA and 1400\AA at redshift 3.4, 4.0 and 4.5, respectively. The average spectral slope of the sample is almost flat, $\langle \beta \rangle = -1.95 \pm 0.4$, so the estimated flux density deviates by only a small amount from the observed i_{775} magnitude (less than 5% on average, $F_{\nu} \sim \lambda^{2-\beta}$).
3. **A1500**: The correction for dust attenuation has been calculated assuming the empirical extinction relation $A1500 = 4.43 + \beta 1.99$, where the spectral index β is derived from the observed $(i_{775} - z_{850})$ color following the prescription of Bouwens et al. (2009b; see also Meurer et al. 1999). This technique has already been employed by several previous studies estimating the SFR density at $z \sim 2\text{-}6$ (e.g., Adelberger & Steidel 2000; Meurer et al. 1999; Bouwens et al. 2006; Stark et al. 2007). The dust correction has also been compared to the values derived from the standard SED fitting of a sub-sample of the 102 LBGs (80% of them) for which we have photometric multi-wavelength coverage from the MUSIC catalog. We refer the reader to Santini et al. (2009) for details of the SED fitting procedures. The median and standard deviation of A1500 from the SED fitting is $0.61^{+0.93}_{-0.61}$, while from the ultraviolet spectral slope it is $0.58^{+0.88}_{-0.58}$ assuming a Calzetti extinction law.
4. **IGM attenuation**: The transmission of the IGM ($T = e^{-\tau_{\lambda}^{\text{IGM}}}$) between the observer

and the source redshift has been inserted by adopting the models $\tau_{\lambda}^{\text{IGM}}$ of IW08 (see previous section).

A Monte Carlo simulation that takes into account all of the above quantities has been performed and is described next. Random IGM transmissions have been associated with each object from the spectroscopic sample (102 galaxies) by extracting from the 10,000 different lines of sight at the closest redshift to the source and convolved with the IB filter. Similarly, a value of the intrinsic ratio of the luminosity density has been extracted randomly from the adopted distribution described above, then a correction for the dust absorption (A1500) has been calculated from the observed color. The f_{esc} has been investigated by inserting various functional behaviors (see next section). An estimate of the flux $(F900)_{\text{obs}}$ is derived from Eq. 3. If the estimated $(F900)_{\text{obs}}$ flux is brighter than the adopted threshold (i.e., the depth of the IB image), then it has been further perturbed according to the error of the image photometry for that flux level. The error as a function of the magnitude has been parameterized analytically by fitting an exponential function to the observed data.

Ten thousand simulated samples of 102 galaxies, each anchored to the observed quantities of the *clean* sample, i.e., the rest-frame ultraviolet colors, magnitudes and redshift, have been generated for each f_{esc} distribution. For each of the 10,000 extractions, the number of sources brighter than the chosen IB magnitude limit is recorded. At the end, for each assumed f_{esc} distribution, 10,000 estimations of the expected number of “survived” sources is calculated, and the median and central 68 percentile range are derived.

Summarizing, the number of expected LyC detections in the IB band has been calculated performing Monte Carlo simulations that take into account the IGM transmission, the IB filter shape, the distribution of the intrinsic luminosity ratio ($L1500/LF_{\text{LyC}}$), dust attenuation by the interstellar medium, photometric errors of the IB image, the observed redshift and i_{775} magnitude.

Once these effects are suitably modeled, the expected number of LyC detections in the IB image depends on the moments of the f_{esc} distribution assumed. The aim of the next section is to investigate these dependencies through comparison with the observed number.

4.3. The tested distributions

It is reasonable to believe that f_{esc} varies from galaxy to galaxy with a distribution currently not known. Indeed, theoretical studies propose various behaviors for f_{esc} as a function of the halo mass, luminosity, gas and dust content, geometry, etc. (Gnedin et al. 2008; Wise & Cen 2009; Yajima et al. 2010; Razoumov & Sommer-Larsen 2010). We

have investigated which effect an assumed distribution of f_{esc} would have on the expected number of LyC detections in our IB image. We assume that the distributions apply for all luminosities.

Before introducing the various functional forms adopted, we perform a similar check to what was done by Siana et al. (2007) in characterizing their null detection of LyC at $z \sim 1.3$. We assume a fraction (Y) of our sample has constant f_{esc} (=X) and the rest (1-Y) has zero LyC emission (X and Y vary between 0 and 1). Monte Carlo simulations have been run in order to estimate the number of expected detections (N) in our IB survey as described in the previous section down to a 2-sigma limit and as a function of X and Y. This has been done 30 times (1000 extractions each) on the clean sample randomly sorted at every time. The results are reported in Figure 16 where points (X,Y) with N=3 belong to the black region; above it N>3 and below N<3. In our sample of 102 LBGs only one has been detected, N=1. Very low f_{esc} (<5%) are needed to reproduce the null or one LyC detection if all LBGs have the same f_{esc} value. Conversely, a high f_{esc} (>70%) can reproduce a null or one detection if it is associated with less than 10% of the LBG sample. This test suggests that high values of f_{esc} are less probable in this luminosity regime (a feature already noted in other works; e.g., Giallongo et al. 2002; Inoue et al. 2005; Shapley et al. 2006; Iwata et al. 2009).

Having this result in mind, various continuous functions have been explored: flat, Gaussian and asymmetric functions (exponential and log-normal). In detail, we test the following functional forms for f_{esc} :

1. **Constant value:** A constant value of f_{esc} has been assumed for all galaxies, between 0.0 and 1.0 with an increment of 0.01. It is not realistic to assume a constant value of f_{esc} . However it is useful as a check of the typical scatter due to solely Monte Carlo simulated effects like IGM, dust, photometric noise, intrinsic luminosity ratio distribution, etc.
2. **Gaussian distribution:** f_{esc} is assumed to be distributed as a Gaussian form with a mean running from 0.0 to 1.0 (step 0.01) and standard deviation equal to half of the mean.
3. **Exponential distribution:** Exponential distributions ($e^{-\lambda}$) with different slopes λ have been considered, with λ running from 1 to 100 with step $\Delta\lambda=1$. This allows us to investigate the effect of asymmetric tails toward high f_{esc} values.
4. **Log-normal distribution:** Log-normal distributions with various medians and scatter have been inserted, $e^{-K+\lambda \times \text{Gauss}}$, where Gauss is extracted randomly from a Gaussian distribution with zero mean and standard deviation equal to 1. K has been

assumed to be 1, 2, 3, 4 and for each λ parameter running from 0.1 to 10.0 (step 0.1). Varying K allows us to change the average of the initial symmetric distribution (small λ). As λ increases, the median of the distribution tends to zero and an asymmetric tail toward high values arises (see below).

In this way 100 constant, Gaussian, exponential and 400 log-normal distributions of f_{esc} have been calculated, each one extracted 10,000 times with the Monte Carlo simulation described above. We discuss the results In the following section.

4.4. Constraints on the ionizing radiation fraction distribution from the spectroscopic sample

The expected number of LyC detections has been explored as a function of the median and 68% interval of the assumed f_{esc} distributions. Figure 17 and 18 show the results for constant, Gaussian and exponential f_{esc} behaviors. As expected, in all cases, if the median f_{esc} increases the number of expected LyC detections also increases. Considering the IB depth at the 2σ level (left panels of Figure 17) and given the single LyC detection, the upper limit on the median f_{esc} is $\simeq 6(5)\%$ at 3σ for the Gaussian (exponential) distribution. Relaxing to a shallower IB depth, 29.1 (3σ) and 28.6 (5σ), the median of the Gaussian (exponential) f_{esc} distribution is lower than 12(10)% and 20(15)%, respectively.

Focusing on the exponential distribution, a median less than $\sim 5\%$ and a scatter less than $\sim 15\%$ are required to be compatible within 3σ to the observations. In other words, the very low number of LyC detections in the IB image down to 29.5 limit (2σ within 1.2'' diameter) implies an upper limit to the median f_{esc} and the 84% percentile of the distribution of 5% and 15%, respectively. Figure 18 shows in more detail the exponential case reported in the lower left panel of Figure 17, i.e., IB depth at 2σ level. In particular, the distributions that lead, on average, to an expected number of LyC detections higher than 4 are highlighted in the [median – scatter] plane (see inner right box of the same figure). Following the Poisson statistics, these are distributions for which the probability to have less than two LyC detections (our case) is lower than 5%.

While in the above cases the dispersion decreases together with the median of the distribution and approaches zero as the median tends to zero, the effect of a relatively high scatter and very small median of f_{esc} has been explored by adopting log-normal distributions as described in the previous section. The case with $K = 1$ and λ running from 0.1 to 10.0 ($\Delta\lambda = 0.1$) is shown in Figure 19. As λ increases, the distribution changes its shape from symmetric and centered at the initial value e^{-1} ($K = 1$) to asymmetric with very small

median and relatively high 84% scatter (see examples in the main box of Figure 19). In the extreme case of very small medians (e.g., $\lambda = 100$, median e^{-100}) the scatter still allows a marginal LyC detection. This is the reason why in Figure 19 the expected number of LyC detections is different from zero even though the median is close to zero. Similarly, for the exponential case, the locus of points in the [median – scatter] plane of all the log-normal distributions (varying λ and $K = 1$) is shown in the inner right box of Figure 19. Those excluded with a probability higher than 95% have been highlighted. In this case, log-normal distributions with a scatter lower than $\sim 18\%$ are favoured if compared with observations. Similar results have been found varying log-normal distributions with $K = 1, 2, 3, 4$ and λ running from 0.1 to 10.0 (see Figure 20).

Summarizing, among the f_{esc} distributions explored and from the comparison with the observed number of LyC detections (i.e., 1 out of 102) we find that the median fraction of ionizing radiation escaping from the LBG sample considered here is less than $\sim 5\text{-}6\%$ with a 1σ scatter (upper eighty-fourth percentile) not larger than $\sim 20\%$ at the 2σ IB depth. These upper limits increase to $\sim 10\text{-}12\%$ and 20% (median and 1σ) if the 3σ IB depth is considered. In general, adopting the Poissonian statistics and considering the single LyC here reported, the distributions that predict more than 5 (10) LyC detections can be excluded with a probability higher than 95%(99%), respectively.

5. Upper limits on the ionizing radiation fraction from stacking

5.1. IB imaging

The median and average stacking of all 102 galaxies are shown in the top part to Figure 21. No LyC detection is seen. Similarly, the median and average stacks have been performed for the sub-sample of 45 LBG with redshift lower than 3.6, for which the mean IGM transmission is higher (see Figure 14). Median and averages have also been calculated for two sub-samples of these 45 galaxies, one of 22 LBG with $i_{775} < 25$ and the other for 23 LBG with $i_{775} > 25$ (they are shown in Figure 21). None of them show a LyC detection. It is worth noting that the individual LyC measure described in Sect. 3.2.1. (when included) does not provide enough counts to contribute to a significant stacked detection.

Following previous work in the literature (e.g., Steidel et al. 2001; Giallongo et al. 2002; Inoue et al. 2005; Shapley et al. 2006; Iwata et al. 2009), an upper limit on the f_{esc} can be calculated by assuming average values for the quantities in Eq. 2 and correcting $f_{\text{esc,rel}}$ for the average dust extinction at 1500\AA . Figure 9 shows the IB flux (AB) distribution within the $1.2''$ aperture of the sample of 102 LBGs plus 6 AGNs. Excluding the AGNs and the single

LBG detected in its LyC, the distribution has a mean and standard deviation of $\langle F(1.2'') \rangle = -0.007 \pm 0.023 \times 10^{-30} \text{ erg sec}^{-1} \text{ cm}^{-2} \text{ Hz}^{-1}$. This one sigma dispersion corresponds to magnitude 30.50 AB, consistently with the one sigma limit described at the beginning, and can be adopted as the typical error of the single measure (assuming the flux distribution to be Gaussian and each measurement as independent). Therefore the one sigma limit of the mean over N sources is $0.023 \times 10^{-30} \text{ erg sec}^{-1} \text{ cm}^{-2} \text{ Hz}^{-1}$ decreased by the square root of N . In the case of 102 LBGs, this limit corresponds to magnitude 33. However, despite the very deep flux reached, the very low transmission of the IGM as redshift increase ($z > 4$) weakens the constraints on f_{esc} . In order to keep a relatively high IGM transmission and high magnitude contrast, galaxies with redshift lower than 3.75 and $i_{775} < 25.5$ have been selected (64 LBGs). The average i_{775} magnitude and redshift are 24.84 and 3.57, respectively, and the observed one sigma flux density ratio probed is $(F_{1500}/F_{\lambda_{\text{rest}}})_{\text{obs}} = 1473$. The upper limit on $f_{\text{esc,rel}}$ is

$$f_{\text{esc,rel}} < \left[\frac{7}{1473} \right] \times \frac{1}{0.09} = 0.05, \quad (4)$$

where the average transmission is $\simeq 0.09$ at redshift below 3.75 (see Figure 14) and the intrinsic luminosity ratio has been fixed to 7 (see previous section). Assuming an average $A_{1500}=0.65$ (flat spectral slope), the upper limit on total escape fraction $f_{\text{esc}} = f_{\text{esc,rel}} \times 10^{-0.4A_{1500}}$ turns out to be 0.03.

Several further constraints on f_{esc} can be calculated by selecting subsamples in magnitude and redshift. Selecting brighter sources allows one to increase the magnitude contrast, and selecting lower redshift sources allows one to increase the average IGM transmission because the IB filter approaches rest-frame 900Å. A summary of this is shown in Table 4 where upper limits on f_{esc} are reported as a function of the magnitude threshold (columns) and redshift (rows). The upper limits on the (mean) escaping ionizing radiation f_{esc} span the range 4% to 60%. The values derived from the Monte Carlo simulations are consistent with this interval, in particular if the brighter (large magnitude contrast) and lower redshift (higher IGM transmission) objects are considered in the grouping (see Table 4). Compared to the estimations appearing in the literature so far, these are the most constraining results on f_{esc} in the redshift and magnitude range here considered.

As discussed at the end of Sect. 4.1, it is worth noting the effect of the recent findings of Prochaska et al. (2010) and Songaila & Cowie (2010) about the lower incidence of LLSs observed with respect to previous work (e.g., Pèroux et al. 2005; also adopted in this work). Assuming these results to be correct, they imply a higher IGM transmission by a factor of 1.5 (this has been done by rescaling the predictions of IW08 to match the number of LLSs reported in those works). Therefore, the limits we report in the above equation would further

decrease by the same factor (Eq. 4). The same dimming factor would also apply to the upper limits reported in Table 4.

5.2. NB imaging

The number of available sources of the *clean* sample in the FORS1 NB imaging is 30. There are two more LBGs in this sample (not considered in the IB calculations) since the NB imaging starts to probe the LyC at redshift beyond 3.3 (not 3.4 as for the IB). None of the LBGs show a LyC detection at $S/N > 2$, and again no detection is measured in the median (average) stacking. While the NB observations have the disadvantage of having smaller statistics and being shallower than the IB imaging, the narrow wavelength window helps to increase the average transmission of the IGM if a suitable selection in redshift is done (the limits calculated from the whole sample do not add any further constraint with respect to the IB derivations). Indeed, selecting sources with redshift below 3.65, the average transmission turns out to be 0.2 and the probed rest-frame wavelengths span the interval 843-890Å. As above, an intrinsic luminosity ratio of $(L_{1500}/L_{\lambda_{\text{rest}}})_{\text{int}} = 7$ is adopted (see Sect. 4.2). Eight galaxies match the selection $3.3 < z < 3.65$ and $i_{775} < 25.5$, with averages $\langle z \rangle = 3.5 \pm 0.1$ and $\langle i_{775} \rangle = 24.6 \pm 0.4$. In the average process the one sigma lower limit of the flux ratio probed (magnitude NB~29) is $F_{1500}/F_{\text{NB}} = 161$, which translates to an upper limit on f_{esc} of 12% assuming an intrinsic ratio of 7 and the same dust extinction A_{1500} adopted for the IB stacking (it is $f_{\text{esc,rel}}$ of 22%). As discussed in the previous section adopting the correction factors for the transmission of Songaila & Cowie (2010) and Prochaska et al. (2010) these limits would be lowered.

6. Evidence for a luminosity dependency?

The limits on f_{esc} derived from Monte Carlo simulations and from the stacking have been calculated from the spectroscopic sample of LBG, which is probing mainly $L \gtrsim L_{z=3}^*$ luminosities, i.e., galaxies hosted by relatively massive dark matter halos ($\simeq 10^{11} M_{\odot}$; e.g., Arnouts et al. 2002, Lee et al. 2009). If we adopt the $z \sim 4$ luminosity function of Bouwens et al. (2007) integrated down to the faint limit $M_{\text{UV}} = -16$ ($0.02 L_{z=3}^*$), the one-sigma limit $f_{\text{esc,rel}} \simeq 5\%$ derived from the brighter part of the sample here analyzed and assumed valid for all luminosities, we find the ionizing background intensity provided by the LBG population

at $z \sim 4$ to be $J_\nu(\text{LyC}) < 0.8 \times 10^{-22} \text{ erg s}^{-1} \text{ Hz}^{-1} \text{ cm}^{-2} \text{ sr}^{-1}$.³ This value represents $\simeq 16\%$ and 19% of the total ultraviolet background intensity measured by Giallongo et al. (1996) and Bolton et al. (2005), respectively, while it increases to 40% of the estimation of Faucher-Giguère et al. (2008b).⁴ If we integrate the luminosity function down to $M_{\text{UV}} = -10$, these fractions increase slightly to 23% , 28% and 56% , respectively. Therefore star-forming galaxies alone may not be able to account for the entire ultraviolet ionizing budget. It is worth noting that, given the observed global non-detection here reported, a higher transmission of the IGM (Prochaska et al. 2010) would imply an even tighter constraint on the escaping radiation and therefore less contribution by (bright) LBGs. If galaxies only partially contribute, the remaining fraction presumably is provided by QSOs. However, several works agree on the fact that at redshift beyond 3, galaxies play a dominant role in the IGM ionization with QSOs contributing fractions of only $30\text{--}10\%$ in the redshift range $3.5\text{--}4.0$, (e.g., Bolton et al. 2005; Siana et al. 2008; Faucher-Giguère et al. 2008b; Faucher-Giguère et al. 2009; Prochaska et al. 2009). If galaxies are responsible for the remaining ionizing budget, then the implication is that f_{esc} depends on the UV luminosity, with fainter galaxies having a larger escape fraction.

Such a relationship between f_{esc} and the UV luminosity has recently been suggested by simulations. Yajima et al. (2010) performed a three-dimensional radiation transfer calculation of stellar radiation for a large number of high-redshift, star-forming galaxies in cosmological simulations. One of their primary conclusions was that, in the redshift interval $3 < z < 6$, galaxies become the main contributor to IGM ionization with the average (standard deviation) of the escape fraction of ionizing radiation increasing to $\simeq 40\%$ (20%) for low mass haloes, $M_h < 10^{10} M_\odot$. For the larger haloes, $M_h \simeq 10^{11} M_\odot$, they predict an average f_{esc} of 7% with a relatively small scatter, less than 20% (see their Figure 2), in agreement with what we find here.

Sources at the fainter end of the magnitude distribution are under-represented in our simulations, since the magnitude contrast reached between the ionizing and non-ionizing radiation (IB and i_{775}) is smaller. However, if there is a dependency of f_{esc} with the

³The ionizing luminosity density $\rho_{\text{LyC}} = \rho(1500) \frac{L_{\text{LyC}}}{L_{1500}}(f_{\text{esc,rel}})$ is independent from the intrinsic luminosity ratio, see Eq. 2.

⁴Bolton et al. (2005) and Faucher-Giguère et al. (2008) calculate the total photoionization rate Γ_{-12} of 1.0 and 0.5, respectively (where $\Gamma_{-12} = \Gamma/10^{-12} \text{s}^{-1}$). We convert these values into intensity units ($\text{erg s}^{-1} \text{ Hz}^{-1} \text{ cm}^{-2} \text{ sr}^{-1}$) by adopting the formulation in Schirber & Bullok (2003): $\Gamma_{-12} = (12/(3 + \alpha_{\text{UV}})) \times J_{-21}$ and assuming an α_{UV} spectral slope of the background intensity equal to 2 (e.g., Haehnelt et al. 2001) and J_{-21} is the intensity of the ultraviolet background in units of $10^{-21} \text{ erg s}^{-1} \text{ Hz}^{-1} \text{ cm}^{-2} \text{ sr}^{-1}$ (see Eq. 7 of Schirber & Bullok 2003).

luminosity so that fainter galaxies have higher average f_{esc} , this could partially compensate for the lower contrast. As mentioned above, Yajima et al. (2010) predicts f_{esc} increases for lower halo masses, with $\langle f_{\text{esc}} \rangle$ of $40 \pm 30\%$ and $15 \pm 20\%$ for $M_h = 10^9 M_\odot$ and $M_h = 10^{10} M_\odot$, respectively. Razoumov & Sommer-Larsen (2010) predict f_{esc} values that reach 70-80% for M_h in the range 10^9 – $10^{10} M_\odot$ at redshift 4.4.

To investigate the IB emission in our data at fainter limits we have selected a sample of 218 galaxies with photometric redshifts in the range $3.4 < z < 4.0$ and magnitude $27 < i_{775} < 28.5$ extracted from the public photometric redshift catalog of Coe et al. (2006). IB photometry has been performed at the positions of the galaxies in the four aperture diameters, as was done for the spectroscopic sample. Twenty-six out of 218 have a detection with S/N ratio higher than 2 in the $1.2''$ diameter aperture; Figure 22 shows their IB cutouts and the list is reported in Table 5. Five out of 26 show an IB emission aligned with the LBG position (marked with black crosses in Figure 22). In the other cases an offset is present and the LBG may suffer contamination by foreground sources.

From Monte Carlo simulations of the sample considered here we find that the expected median number of LyC detections at the 2σ IB depth is 6_{-2}^{+3} and 3_{-1}^{+2} for the case of constant and Gaussian distributions with median $f_{\text{esc}}=1.0$ and 0.7 , respectively. Exponential and log-normal distributions predicts a comparable number ($\simeq 3 - 6$) if the median of the f_{esc} distributions is larger than 60%. This result is quantitatively consistent with the expectations if f_{esc} increases for less luminous galaxies.

However, we stress that apart from the reduced magnitude contrast probed, the main disadvantage concerning these fainter sources is the reliance on photometric redshifts. If the sample includes some galaxies with true redshifts $z < 3.4$, the IB image would include light from wavelengths longward of the Lyman limit.

7. Conclusions

Exploiting the ultra-deep VIMOS IB and deep FORS1 NB imaging of the GOODS-South field, new limits on the escape fraction of ionizing radiation from star-forming galaxies at redshift 3.4–4.5 have been derived. Particular care has been devoted to clean the spectroscopic sample from foreground contamination and AGN contributions. From a sample of 102 LBGs we derive the following results:

1. From Monte Carlo simulations and stacking of the IB and NB imaging, we find that f_{esc} of $L \geq L_{z=3}^*$ LBG is distributed with a median lower than 5-6% and 84 percentile scatter lower than 20% in all the distributions investigated (Gaussian, exponential and

log-normal). We note that the low upper limit on the median escape fraction is for the entire sample, independent of spectral properties. If the recent findings of Prochaska et al. (2010) and Songaila & Cowie (2010) are considered — i.e., the average IGM transmission is higher than that adopted here — then the limits we derive are further strengthened.

2. One star-forming galaxy is detected in its LyC region at 700–835Å rest-frame. It is the highest redshift galaxy with such a detection currently known and is most probably due to a combination of high IGM transmission coupled with a relatively high f_{esc} . The lower limit on f_{esc} is 15%; assuming $f_{\text{esc}}=100\%$, the IGM transmission cannot be lower than 15%. This value is higher than the expected average value at this redshift (2.2%), implying that it is a particularly free line of sight. The galaxy shows a blue UV–continuum spectral slope ($\beta=-2.1$) and weak or absent interstellar absorption lines in the spectrum even though Ly α is in absorption. The ultraviolet morphology is quite compact, $R_{\text{eff}}=0.8$ kpc (physical).

Adopting the observed photoionization rate of Bolton et al. (2005) or Faucher-Giguère et al. (2008b), star-forming galaxies contribute partially ($\lesssim 50\%$) to the required ultraviolet ionizing budget if f_{esc} is constant and equal to 5%. On one hand, the contribution of QSOs may still be significant at the redshifts considered here, providing the ionizing fraction missed by galaxies. This strongly depends on the faint-end slope of the QSO luminosity function (Glikman et al. 2010, and in preparation). On the other hand, several works suggest that the QSO contribution to the UVB decreases significantly beyond redshift 2, reaching fractions lower than 50% (down to 10%) at redshift 4 (e.g., Fontanot et al. 2007; Siana et al. 2008; Faucher-Giguère et al. 2008b; Prochaska et al. 2009). In this case galaxies would provide almost all of the ionizing radiation, which, as we have seen, requires that f_{esc} depends on the UV luminosity. We remind, however, that these conclusions depend on both the total ionizing UVB and the QSO fractional contribution to it, quantities remain empirically poorly constrained at these redshifts.

If f_{esc} does indeed depend on the UV luminosity, then we can speculate on the following scenario. Bouwens et al. (2009b), analyzing samples of LBGs in the redshift range $3 < z < 6$ show that there is a clear correlation between the UV–continuum slope β and ultraviolet luminosity. In particular, for the B –band dropout sample also adopted here, more luminous LBGs have redder colors. Moreover, it is known from stacking tens and hundreds of LBG spectra at redshift 3–5 that the redder UV–continuum slopes are linked to low Ly α equivalent widths and stronger interstellar absorption lines, while Ly α emitters are bluer and have weaker interstellar absorption lines (e.g., Shapley et al. 2003; Pentericci et al. 2007; Vanzella et al. 2009; Balestra et al. 2010).

Thus, if f_{esc} is, on average, larger in galaxies with fainter UV luminosity then we would expect that the bulk of the ionizing radiation comes from faint Ly α emitters, which are, in general, younger and less massive than their brighter LBG counterparts (e.g., Ono et al. 2010). On the one hand, this would be plausible and possible cases have been found by Iwata et al. (2009). On the other hand, we have shown an opposite example, in which LyC emission arises from a LBG without Ly α in emission (even though it has been detected in the bright $L_{z=3}^*$ regime).

A direct investigation at fainter flux limits ($i_{775} > 27$) is challenging because the magnitude contrast decreases and spectroscopic redshifts are difficult to obtain with current facilities. An analysis of faint galaxies from the HUDF, $27 < i_{775} < 28.5$ or $0.3L_{z=3}^* - 0.04L_{z=3}^*$, selected with photometric redshift is in broad quantitative agreement with the expectations if f_{esc} depends on the UV luminosity, increasing for fainter galaxies.

A way to explore this faint luminosity regime (before the advent of future telescopes like *JWST* and the ELTs) is to analyze samples of spectroscopically confirmed LAEs selected through NB imaging (e.g., Iwata et al. 2009; Inoue et al. 2010), looking at peculiar spectroscopic features related to low-luminosity AGN or hot and massive stars (e.g. Vanzella et al. (2010a)) or using spectra of γ -ray burst afterglows (e.g., Chen et al. 2007), strategies that we plan to pursue in upcoming works.

We would like to thank the anonymous referee, whose comments improved the paper. We are grateful to the ESO staff in Paranal and Garching who greatly helped in the development of this programme. We acknowledge financial contribution from contract ASI/COFIN I/016/07/0 and PRIN INAF 2007 “A Deep VLT and LBT view of the Early Universe”. We would like to thank D. Schaerer for useful discussions about the single LBG detection and E. Glikman for the recent estimates of the QSO luminosity function at the faint end at redshift 4. The work of DS was carried out at Jet Propulsion Laboratory, California Institute of Technology, under a contract with NASA.

REFERENCES

- Adelberger & Kurt L., Steidel, Charles C., 2000, ApJ, 544, 218
- Arnouts, S., Moscardini, L., Vanzella, E., Colombi, S., Cristiani, S., Fontana, A., et al., 2002, MNRAS, 329, 355
- Balestra, I., Mainieri, V., Popesso, P., Dickinson, M., et al., 2010, A&A, 512, 12

- Beckwith, S. V. W., et al. 2006, AJ, 132, 1729
- Bertin, E., Arnouts, S., 1996, A&A, 117, 393
- Bouwens, R. J., Illingworth, G. D., Blakeslee, J. P., Franx, M., 2006, ApJ, 653, 53
- Bouwens, R. J., Illingworth, G. D., Franx, M.; Chary, R.-R., et al., 2009, ApJ, 705, 936
- Bouwens, R. J., Illingworth, G. D., Oesch, P. A., et al., 2010, ApJ, 709, 133
- Bouwens, R. J., Illingworth, G. D., Oesch, P. A., Labbe, I., et al., 2010, submitted to ApJ, (arXiv/1006.4360)
- Bruzual, G., Charlot, S., 2003, MNRAS, 344, 1000
- Calzetti, Daniela, Armus, Lee, Bohlin, Ralph C., Kinney, Anne L., Koornneef, Jan, Storchi-Bergmann, Thaisa, 2000, ApJ, 533, 682
- Castellano, M., Fontana, A., Boutsia, K., Grazian, A., Pentericci, L., Bouwens, R., et al., 2010, A&A, 511, 20
- Cen, Renyue & Haiman, Zoltan, 2000, ApJ, 542, 75
- Chen, Hsiao-Wen, Prochaska, Jason X., Gnedin, Nickolay Y., 2007, ApJ, 667, 125
- Coe D., Benitez, N., Sánchez, S. F., et al., 2006, AJ, 132, 926
- Cowie, L. L., Barger, A. J., Trouille, L., 2009, ApJ, 692, 1476
- Cristiani, S., Appenzeller, I., Arnouts, S. et al., 2000, A&A, 359, 489
- D’Odorico, V., Bruscoli, M., Saitta, F., Fontanot, F., et al., 2008, MNRAS, 389, 1727
- Fan, Xiaohui, Narayanan, Vijay K., Strauss, Michael A., et al., 2002, ApJ, 123, 1247
- Faucher-Giguère, Claude-André, Lidz, Adam, Hernquist, Lars, Zaldarriaga, Matias, 2008, ApJ, 682, 9
- Faucher-Giguère, Claude-André, Lidz, Adam, Hernquist, Lars, Zaldarriaga, Matias, 2008, ApJ, 688, 85
- Faucher-Giguère, Claude-André; Lidz, Adam; Zaldarriaga, Matias; Hernquist, Lars, 2009, ApJ, 703, 1416
- Finkelstein, Steven L., Papovich, Casey, Giavalisco, Mauro, Reddy, Naveen A., Ferguson, Henry C., Koekemoer, Anton M., Dickinson, Mark, 2010, ApJ, in press

- Fontanot, F., Cristiani, S., Monaco, P., Nonino, M., Vanzella, E., et al., 2007, *A&A*, 461, 39
- Giallongo, E., Cristiani, S., D’Odorico, S., Fontana, A., Savaglio, S., 1996, *ApJ*, 466, 46
- Giallongo E., Cristiani S., D’Odorico S., et al., 2002, *ApJ*, 568, 9
- Giavalisco, M., Ferguson, H. C., Koekemoer, A. M., Dickinson, M., Alexander, D. M., Bauer, F. E., Bergeron, J., et al. 2004, *ApJ*, 600, L93
- Glikman, Eilat, Bogosavljevic, Milan, Djorgovski, S. G., Stern, Daniel, et al., 2010, *ApJ*, 710, 1498
- Gnedin, N. Y., Kravtsov, A. V., Chen, H., *ApJ*, 672, 765
- Grazian, A., Fontana, A., de Santis, C., Nonino, M., Salimbeni, S., Giallongo, E., Cristiani, S., Gallozzi, S., Vanzella, E., 2006, *A&A*, 449, 951
- Hayes, Matthew, Ostlin, Goran, Schaerer, Daniel, Mas-Hesse, J. Miguel, 2010, *Nature*, 464, 562
- Hopkins, P. F., Richards, G. T., & Hernquist, L. 2007, *ApJ*, 654, 731
- Inoue, A. K., Iwata, I., Deharveng, J.-M., Buat, V., Burgarella, D., 2005, *A&A*, 435, 471
- Inoue, Akio K., Iwata, Ikuru, 2008, *MNRAS*, 387, 1681
- Inoue, Akio K., Kousai, K., Iwata, I., Matsuda, Y., et al., 2010, *MNRAS* submitted
- Iwata, I., Inoue, A. K., Matsuda, Y., et al., 2009, *ApJ*, 692, 1287
- Kim, T.-S., Carswell, R. F., Cristiani, S., et al., 2002, *MNRAS*, 335, 555
- Lee, K.-S., Giavalisco, M., Conroy C., Wechsler, R.H., Ferguson, H.C., Somerville, R.S., Dickinson, M.E., & Urry, C.M. 2009, *ApJ*, 695, 368
- Leitherer, Claus, Schaerer, Daniel, Goldader, Jeffrey D., et al., 1999, *ApJ*, 123, 3
- Luo, B., Bauer, F. E., Brandt, W. N., Alexander, D. M., et al., 2008, *ApJ*, 179, 19
- Meiksin, Avery, 2006, *MNRAS*, 365, 807
- Meurer, Gerhard R., Heckman, Timothy M., Calzetti, Daniela, 1999, *ApJ*, 521, 64
- Oke, J.B., 1974, *ApJS*, 27, 21

- Péroux, Cléine, Dessauges-Zavadsky, Miroslava, D’Odorico, Sandro, Sun Kim, Tae, McMahon, Richard G., 2005, MNRAS, 363, 479
- Komatsu, E., Smith, K. M., Dunkley, J., et al., 2010, submitted to Astrophysical Journal, (arXiv:1001.4538)
- Malkan, M., Webb, W., Konopacky, Q., 2003, ApJ, 598, 878M
- Nonino, M., Dickinson, M., Rosati, P., et al., 2009, ApJ, 183, 244
- Ono, Yoshiaki, Ouchi, Masami, Shimasaku, Kazuhiro, Akiyama, Masayuki, et al., 2010, MNRAS, 402, 1580
- Pentericci, L., Grazian, A., Fontana, A., Salimbeni, S., Santini, P., de Santis, C., Gallozzi, S., Giallongo, E., 2007, A&A, 471, 433
- Pentericci, L., Grazian, A., Scarlata, C., Fontana, A., Castellano, M., Giallongo, E., Vanzella, E., 2010, A&A, 514, 64
- Popesso, P., Dickinson, M., Nonino, M., Vanzella, E., Daddi, E., et al., 2009, A&A, 494, 443P
- Prochaska, J. Xavier, Worseck, Gabor, O’Meara, John M., 2009, ApJ, 705, 113
- Razoumov, A. O., Sommer-Larsen, J., 2010, ApJ, in press (arXiv:0903.2045)
- Santini, P., Fontana, A., Grazian, A., Salimbeni, S., Fiore, F., Fontanot, F., et al., 2009, A&A, 504, 751
- Schirber, Michael, Bullock, James S., 2003, ApJ, 584, 110
- Shapley, A.E., Steidel, C.C., Pettini, M., Adelberger, K.L., 2003, ApJ, 588, 65
- Shapley, A. E., Steidel, C. C., Pettini, M., Adelberger, K. L., & Erb, D. K. 2006, ApJ, 651, 688
- Siana, B., Teplitz, H. I., Colbert, J., et al., 2007, ApJ, 668, 62S
- Siana, Brian, Polletta, Maria del Carmen, Smith, Harding E., Lonsdale, Carol J., et al., 2008, ApJ, 675, 49
- Siana B., Teplitz H.I, Ferguson H. C., Brown T. M., et al., 2010, ApJ, in press
- Stark, D. P., Bunker, A. J., Ellis, R. S., Eyles, L. P., Lacy, M., 2007, 659, 84

- Steidel, C. C., Pettini, M., & Adelberger, K. L. 2001, *ApJ*, 546, 665
- Szokoly, G. P., Bergeron, J., Hasinger, G., et al., 2004, *ApJ*, 155, 271
- Vanzella, E., Cristiani, S., Dickinson, M., et al., 2006, *A&A*, 454, 423
- Vanzella, E., Cristiani, S., Dickinson, M., Giavalisco, M., et al., 2008, *A&A*, 478, 83
- Vanzella, E., Giavalisco, M., Dickinson, M., et al., 2009, *ApJ*, 695, 1163
- Vanzella, E., Grazian, A., Hayes, M., Pentericci, L., Schaerer, D., Dickinson, M., Cristiani, S., Giavalisco, M., Verhamme, A., Nonino, M., Rosati, P., 2010a, *A&A*, 513, 20
- Vanzella, E., Siana, B., Cristiani, S., Nonino, M., 2010b, *MNRAS*, 404, 1672
- Wise, John H., Cen, Renyue, 2009, *ApJ*, 693, 984
- Yajima, Hidenobu, Choi, Jun-Hwan, Nagamine, Kentaro, 2010, submitted to *MNRAS*, (arXiv:1002.3346)

A. The sources in the extended GOODS-South region

The ESO/VIMOS spectroscopic survey extends beyond the deep GOODS-South area, but where the IB photometry is still available. Thirteen galaxies with secure redshifts match the selection $3.4 < z < 4.5$. Three out of 13 show an IB detection with $S/N \simeq 2.5$. In all three cases the IB emission is offset with respect to the position of the LBG. High-resolution imaging (*HST*/ACS) drawn from the Galaxy Evolution from Morphology and SEDs project (GEMS, Rix et al. 2004) have been used to check for the presence of close companions that may contaminate the IB photometry. Even though the GEMS survey is shallower than GOODS, in all cases there is a distinct faint source shifted in the direction consistent with the IB emission (Figure 6 shows the *HST*/ACS color (V_{606} and z_{850} combined), the VIMOS IB and *R* images, where the deep *R* data are described in Nonino et al. 2009). In particular for the source J033156.8-275151.9 (top panel), a distinct compact source at $\sim 0.6''$ separation from the LBG is clearly present (marked with dotted lines in the Figure). In this case a signal bluer than the Lyman limit is also visible in the two dimensional spectrum (see Figure 23). There is no spatial offset between the two traces in the spectrum because of the slit orientation over the sky superposes the two objects along the wavelength dispersion. It

is further confused by the seeing conditions during the observations ($\sim 1''$). No additional spectral features, possibly arising from the close source, have been detected. In the other two cases (middle and bottom panels of Figure 6) a similarly offset and faint close source is present that can be linked to the contamination.

Table 1. Aperture magnitude limits of the IB VIMOS and NB FORS1 surveys in the GOODS-South.

Depth	<i>U</i> -VIMOS	NB-FORS1
5σ	28.6	27.1
1σ	30.5	29.0

Note. — Magnitudes are reported within aperture diameters of $1.2''$.

Table 2. Summary of the sources adopted.

N	AGNs [N/Detect/Cont]	LBG [N/Detect/Cont]	isolated LBG
122 GOODS-South	7/3/1	115/1/23	92
13 Ext GOODS-South	0/0/0	13/0/3	10
135 Total	7/3/1	128/1/26	102

Note. — [N/Detect/Cont] indicates the number of sources (N), the number LyC detections (Detect) and the number affected by nearby sources (Cont). “Ext GOODS-South” indicates the extended GOODS-South region.

Table 3. The spectroscopic sample of galaxies with a detection in the IB image with $S/N > 2$ in $1.2''$ diameter aperture.

GOODS ID	S/N $1.2''$	S/N $2.1''$	i_{775}	$i_{775} - z_{850}$	zspec	β	comment
J033204.94-274431.7	2.1	7.2	23.71	0.019	3.462 ^{d,b}	-1.9	AGN, NV, CIV; X-ray No
J033216.64-274253.3	5.2	4.4	24.86	-0.015	3.795 ^c	-2.1	LBG, SiIV, CIV (abs); X-ray No
J033238.76-275121.6	3.3	3.4	26.09	0.11	3.951 ^{f,a}	-1.5	AGN, CII,CII[,CIV; X-ray Yes
J033244.31-275251.3	2.9	2.0	23.89	-0.11	3.466 ^{c,e}	-2.6	AGN, NV, SiIV; X-ray Yes

^aFrom Vanzella 08, 09.

^bGOODS VIMOS/LRB, P08, B10.

^cStern et al. in preparation.

^dCristiani et al. 2000, A&A, 355, 485, multiple zspec.

^eSzokoly et al. 2004, ApJS, 155, 271.

^fSpectrum re-analyzed, new redshift measure: CIV, CIII, Ly α .

Table 4. Upper limits on $f_{\text{esc,rel}}$ from stacking.

$i_{775} < 24.75$	$i_{775} < 25.0$	$i_{775} < 25.25$	$i_{775} < 25.5$	$i_{775} < 25.75$	redshift	$\langle T \rangle$
0.051(10)	0.047(17)	0.045(26)	0.045(28)	0.046(30)	[3.40–3.55]	0.135
0.136(17)	0.130(21)	0.127(38)	0.127(36)	0.127(37)	[3.55–3.75]	0.050
0.058(27)	0.054(38)	0.052(56)	0.053(64)	0.053(67)	[3.40–3.75]	0.090
1.208(3)	1.012(6)	0.994(7)	0.994(9)	1.006(10)	[3.75–4.05]	0.013

Note. — The one sigma limits on $f_{\text{esc,rel}}$ values are reported as a function of redshift and magnitude bins. The average IGM transmission $\langle T \rangle$ in the middle of the redshift range and convolved with the IB VIMOS filter, the intrinsic luminosity ratio $L_{1500}/L_{LyC}=7$ are adopted. The total f_{esc} ($f_{\text{esc}} = f_{\text{esc,rel}} \times 10^{-0.4 \times A_{1500}}$) can be obtained by assuming the average dust absorption of the sample, $A_{1500} \simeq 0.65$ (see text). Within parenthesis the number of sources used in the calculation having magnitude less than the corresponding column head and belonging to the redshift interval (*redshift* column). These limits are further decreased by a factor 1.5 if the recent results of Prochaska et al. (2010) and Songaila & Cowie (2010) on the LLSs statistics are considered (see text).

Table 5. Galaxies in the HUDF with photometric redshift in the range 3.4–4.0 and $27 < i_{775} < 28.5$ with a detection in the IB image with $S/N > 2$ in the $1.2''$ aperture.

ID	GOODS ID	zphot	i_{775}	S/N 1.2''	S/N 2.1''
1	J033229.90-274721.5	3.559	28.10	4.6	7.0
2	J033230.79-274740.6	3.495	27.63	3.6	10.1
3	J033232.09-274726.9	3.777	27.21	2.7	5.5
4	J033232.83-274630.0	3.619	27.78	3.6	11.0
5	J033234.63-274819.4	3.487	27.78	2.4	1.8
6	J033236.50-274550.8	3.650	27.80	2.9	3.5
7	J033236.67-274802.9	3.764	27.83	2.2	7.6
8	J033236.67-274743.4	3.681	27.85	4.7	14.0
9	J033236.94-274757.5	3.507	28.43	2.6	5.9
10	J033237.87-274552.9	3.562	27.21	3.7	7.2
11	J033238.30-274728.7	3.488	28.15	3.8	5.6
12	J033238.50-274902.6	3.592	28.03	9.2	9.5
13	J033239.43-274956.6	3.546	28.36	2.6	5.0
14	J033240.70-274936.8	3.830	27.05	3.1	9.4
15	J033240.85-274912.0	3.699	27.91	4.4	6.1
16	J033241.33-274548.2	3.425	28.23	4.6	9.4
17	J033241.57-274604.1	3.497	27.93	3.8	4.2
18	J033241.57-274821.2	3.640	28.35	3.2	8.4
19	J033241.83-274811.9	3.401	27.59	2.7	5.2
20	J033241.86-274718.2	3.509	28.38	2.9	6.6
21	J033242.24-274859.4	3.460	27.57	21.0	33.9
22	J033242.77-274618.1	3.416	28.45	2.9	5.5
23	J033242.89-274845.7	3.761	28.19	3.5	3.2
24	J033244.14-274737.7	3.780	28.45	2.0	3.9
25	J033246.03-274752.8	3.854	27.98	2.4	2.9
26	J033246.97-274730.5	3.610	27.15	4.4	7.3

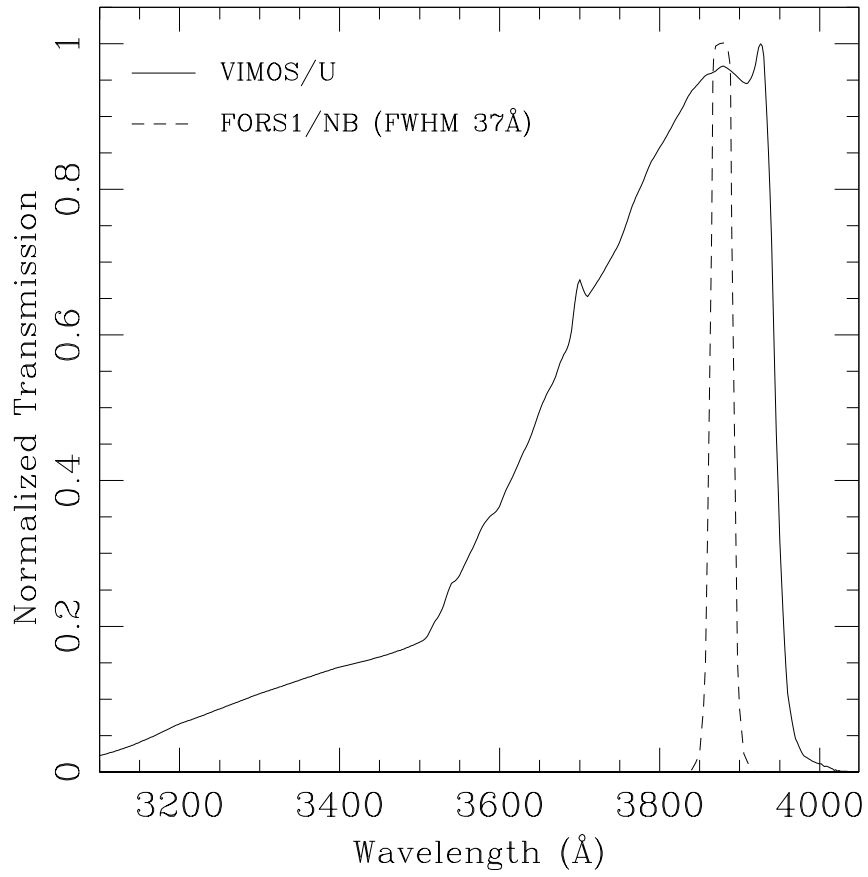


Fig. 1.— Normalized transmissions of the VIMOS/*U* and narrow-band FORS1/3880 filters.

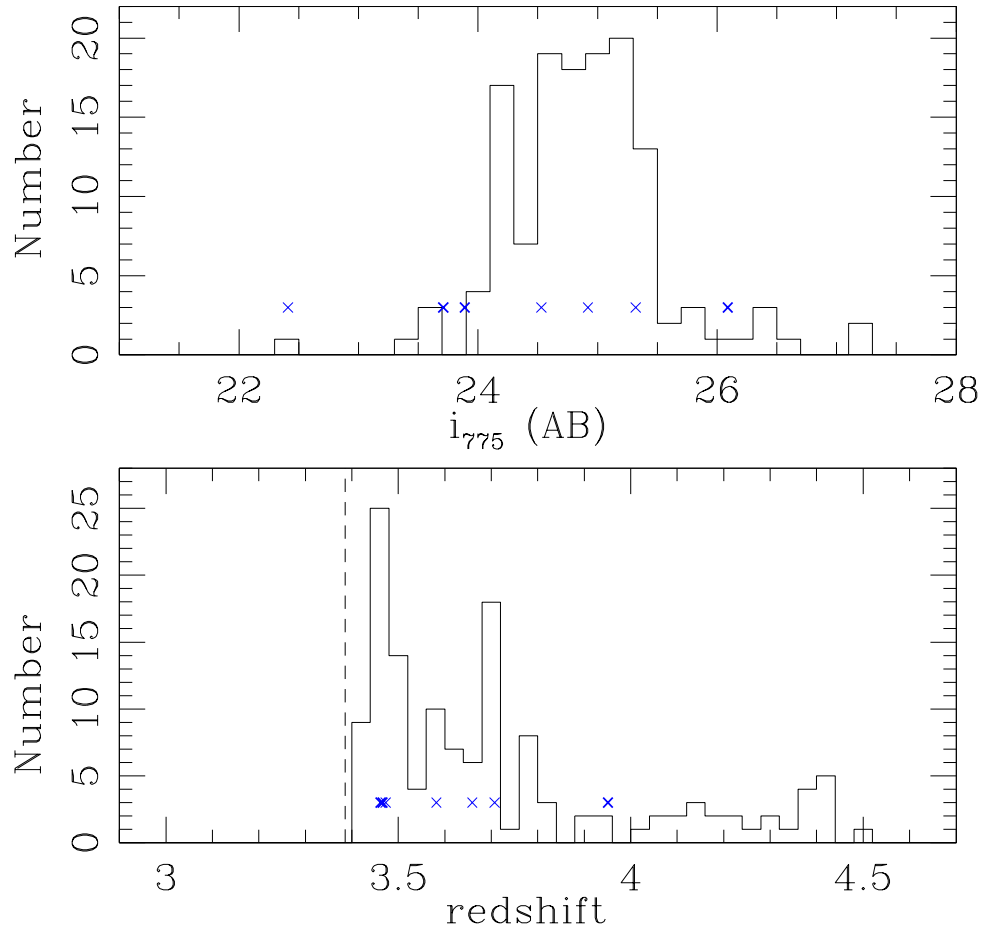


Fig. 2.— Magnitude (top) and redshift (bottom) distributions of the 135 sources considered in this paper (7 AGNs and 128 galaxies). The vertical dotted line in the bottom panel illustrates the minimum redshift probed by the IB for the 912Å limit. In both panels blue crosses mark the AGNs. Those detected in their Lyman continuum are indicated in bold face (see also Figure 8).

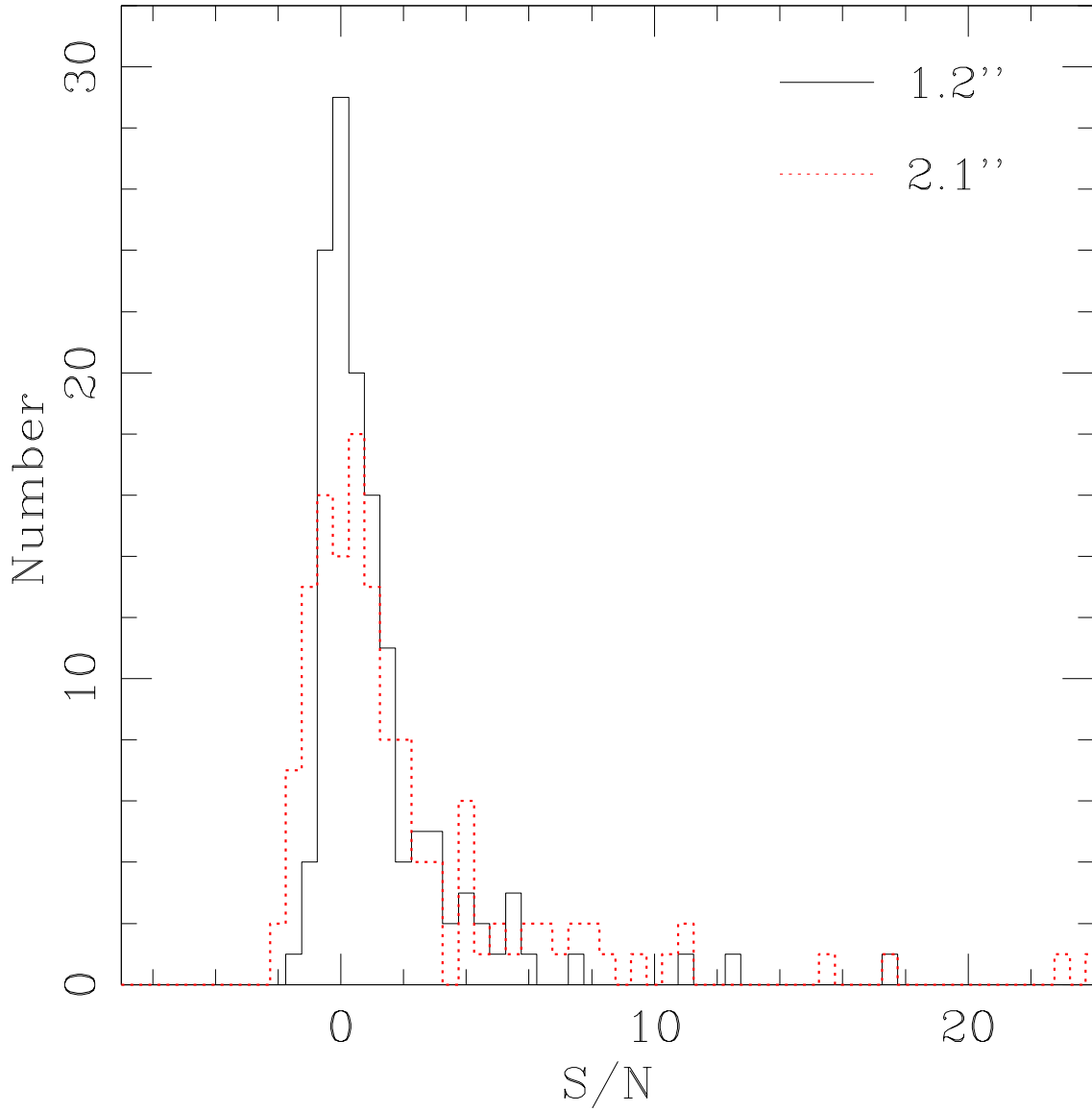


Fig. 3.— IB signal-to-noise ratio distributions calculated for the sample of 135 sources (7 AGNs and 128 galaxies). Two out of four apertures are shown, 1.2'' (solid-black line) and 2.1'' (dotted-red line). The maximum of the distributions peak around zero with a positive tail mainly due to intercepted foreground sources that fall partially in the aperture.

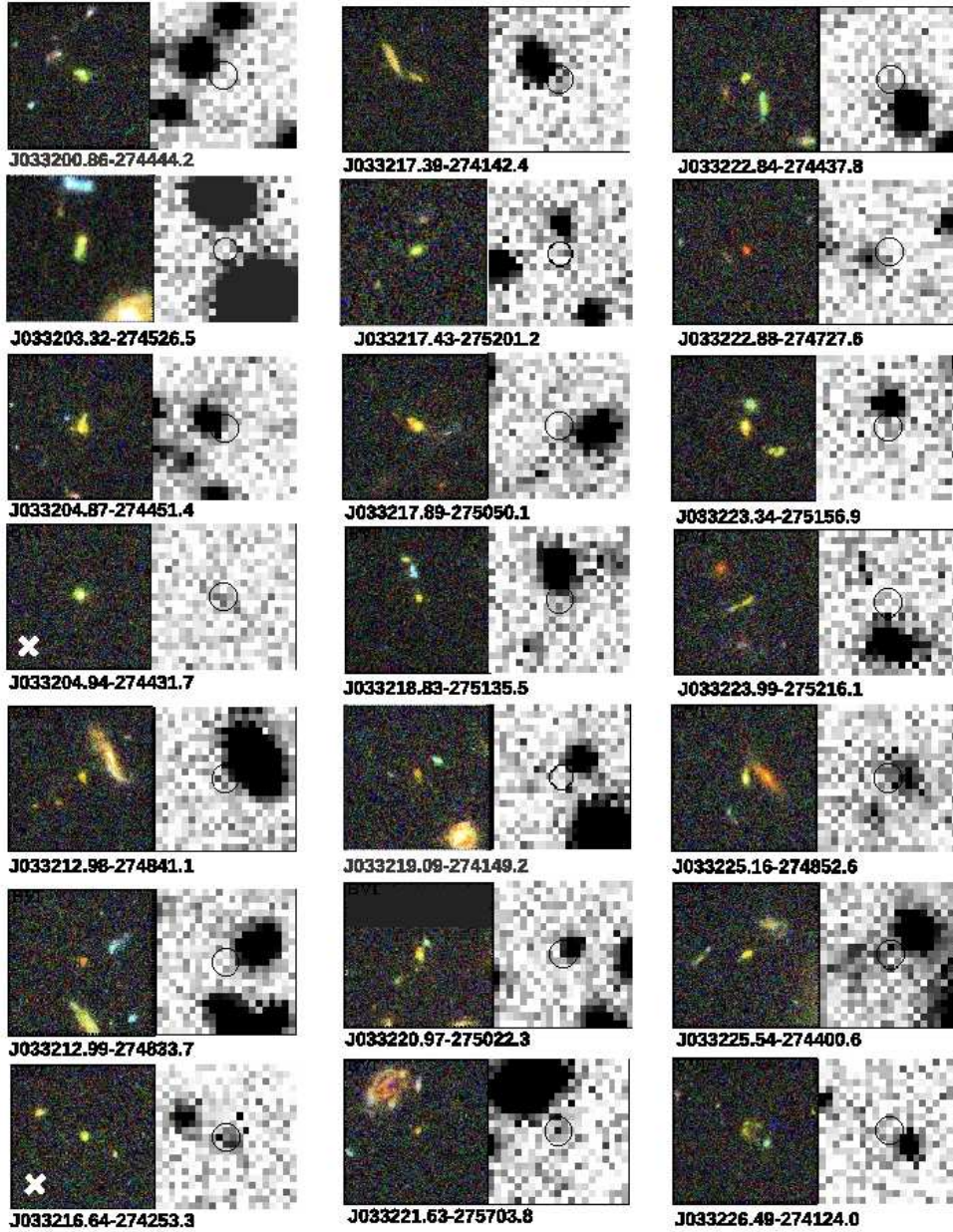


Fig. 4.— The *HST/ACS* *BVi* color images and the ultra-deep *VLT/VIMOS* *IB* cutouts are shown for the sample with a detection above two sigma in the 1.2'' or 2.1'' apertures. The box sizes are 6.3'' on a side and the circles show the 1.2'' diameter aperture. Sources with a white cross are detected in the LyC region; the *IB* detections for the other sources are all considered due to offset foreground contamination.

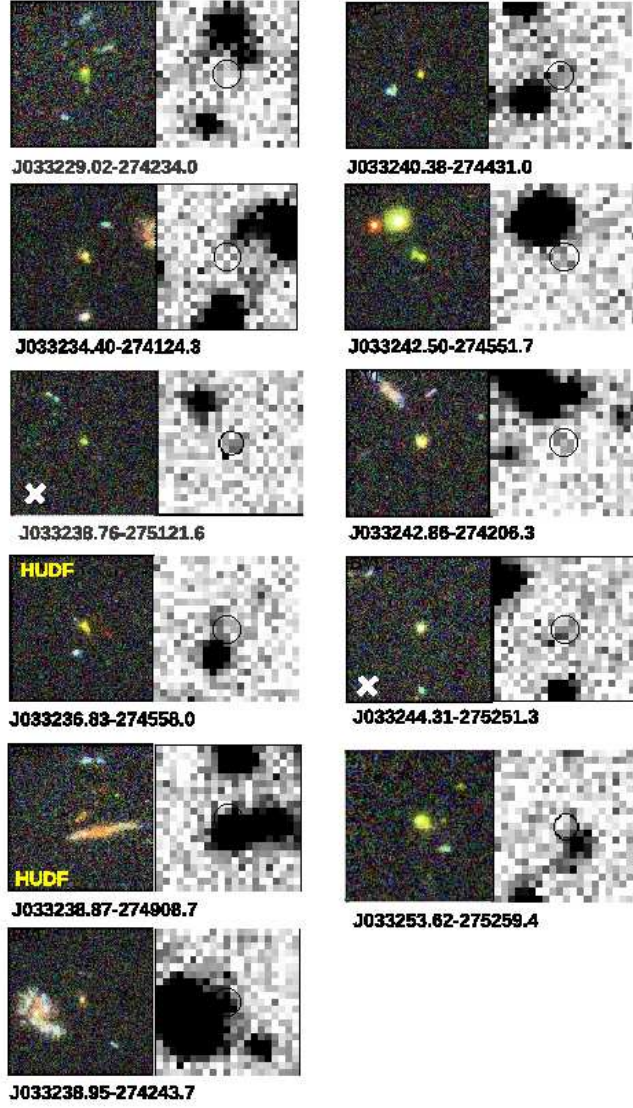


Fig. 5.— The same as Figure 4. Objects belonging to the HUDF are indicated in the BVi cutouts and are shown at the HUDF depth in Figure 7.

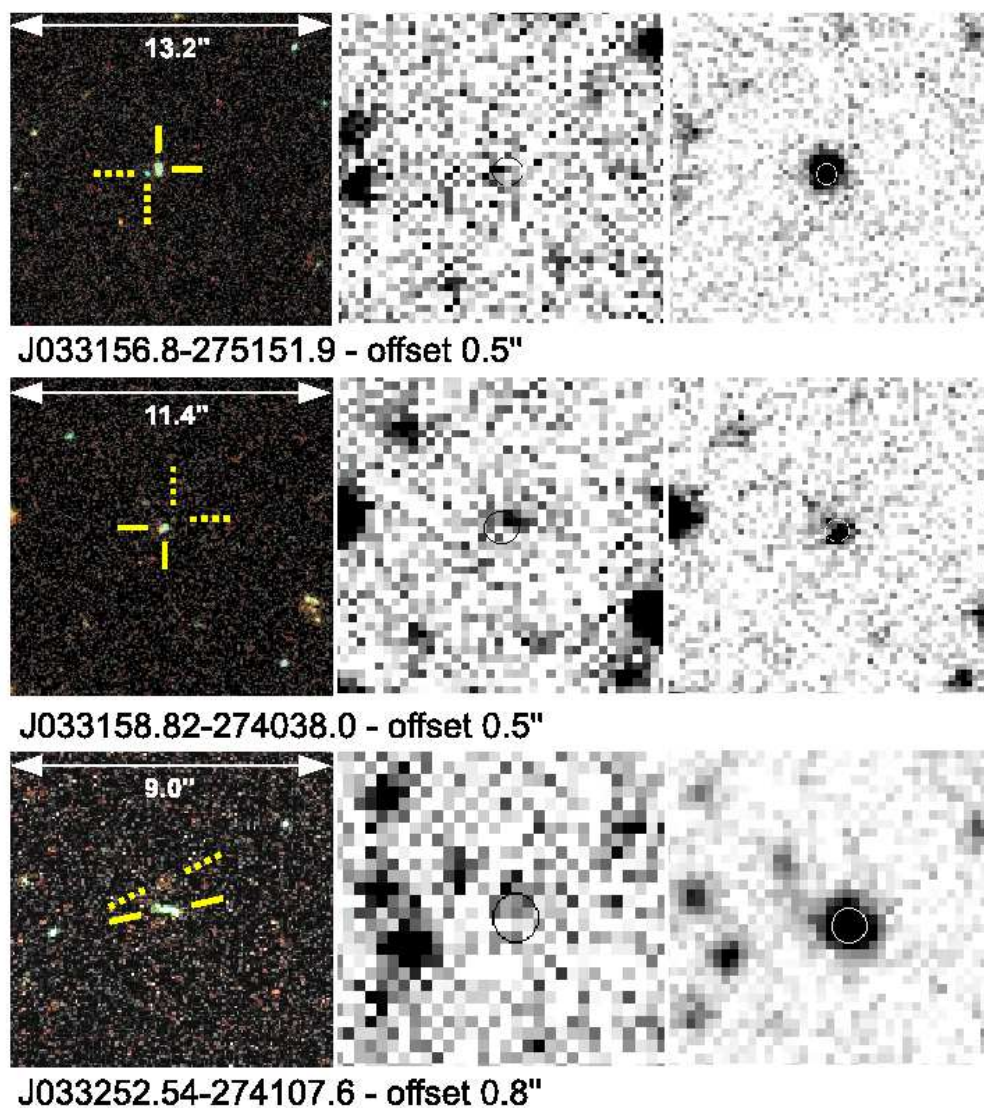


Fig. 6.— Images of the three $z > 3.4$ LBGs outside the ACS GOODS-South area with offset IB detections ($S/N \sim 2.5$). From left to right, ACS two-color images (from GEMS), IB and VIMOS R -band images are shown. The dotted and solid lines indicate the possible nearby polluting source and the targeted LBG, respectively. In all three cases the offset emission in the IB is consistent with the presence of a close source visible in the ACS images. In the middle U -band images, black circles outline the 1.2" diameter apertures, while in the R -band images white circles indicate the position of the spectroscopic target. Below the images, to the right of the GOODS ID, the separation between the LBG and the nearby source is reported. The spectrum of the top source is presented in Figure 23.

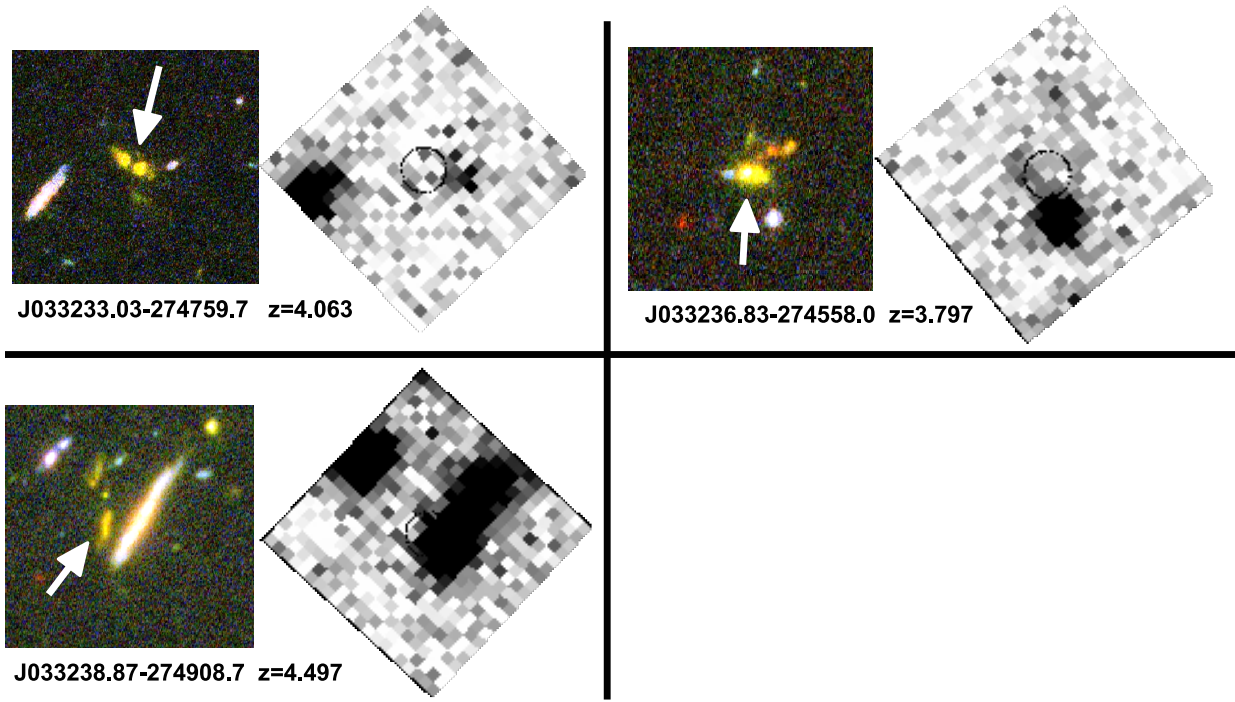


Fig. 7.— Three LBGs in the HUDF detected at $S/N > 1$ ($1.2''$ diameter) in the IB image. The BVi color images at the HUDF depth are shown on the left of each panel. The position of the LBG is marked with a solid arrow in the color image and a circle in the IB (black/white) image. Blue compact sources detected in the IB images are visible, both close to the LBG and in the field. The box size of the IB cutouts is $6''$ on a side.

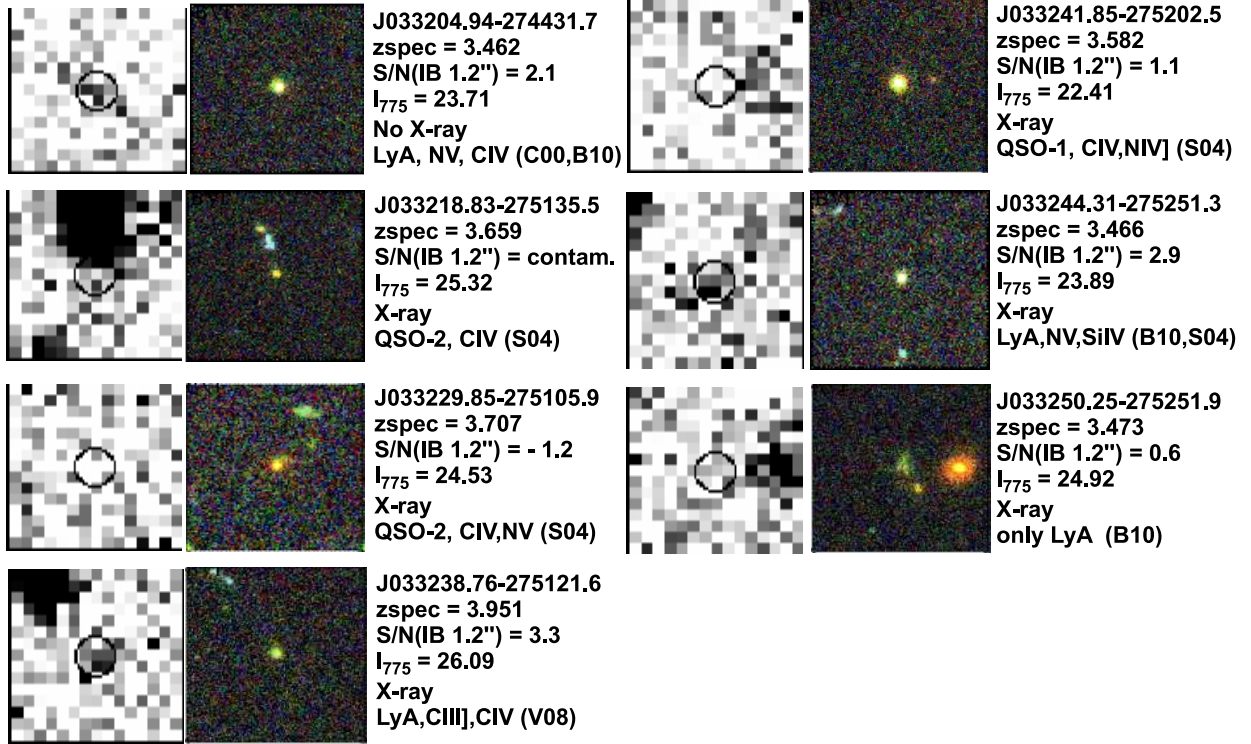


Fig. 8.— *HST*/ACS *BVi* color images and the ultra-deep VLT/VIMOS IB cutouts for the seven AGNs with spectroscopic redshift higher than 3.4. The circles in the IB images have 1.2'' diameters and the box sizes are 4.5'' on a side. For each pair the GOODS ID, redshift, S/N ratio within the 1.2'' diameter aperture, i_{775} magnitude, and the information on the X-ray detection and spectral properties are reported. C00, B10, S04, V08 correspond to Cristiani et al. (2000), Balestra et al. (2010), Szokoly et al. (2004) and Vanzella et al. (2008), respectively. Three out of seven AGNs show a LyC detection at $S/N > 2$.

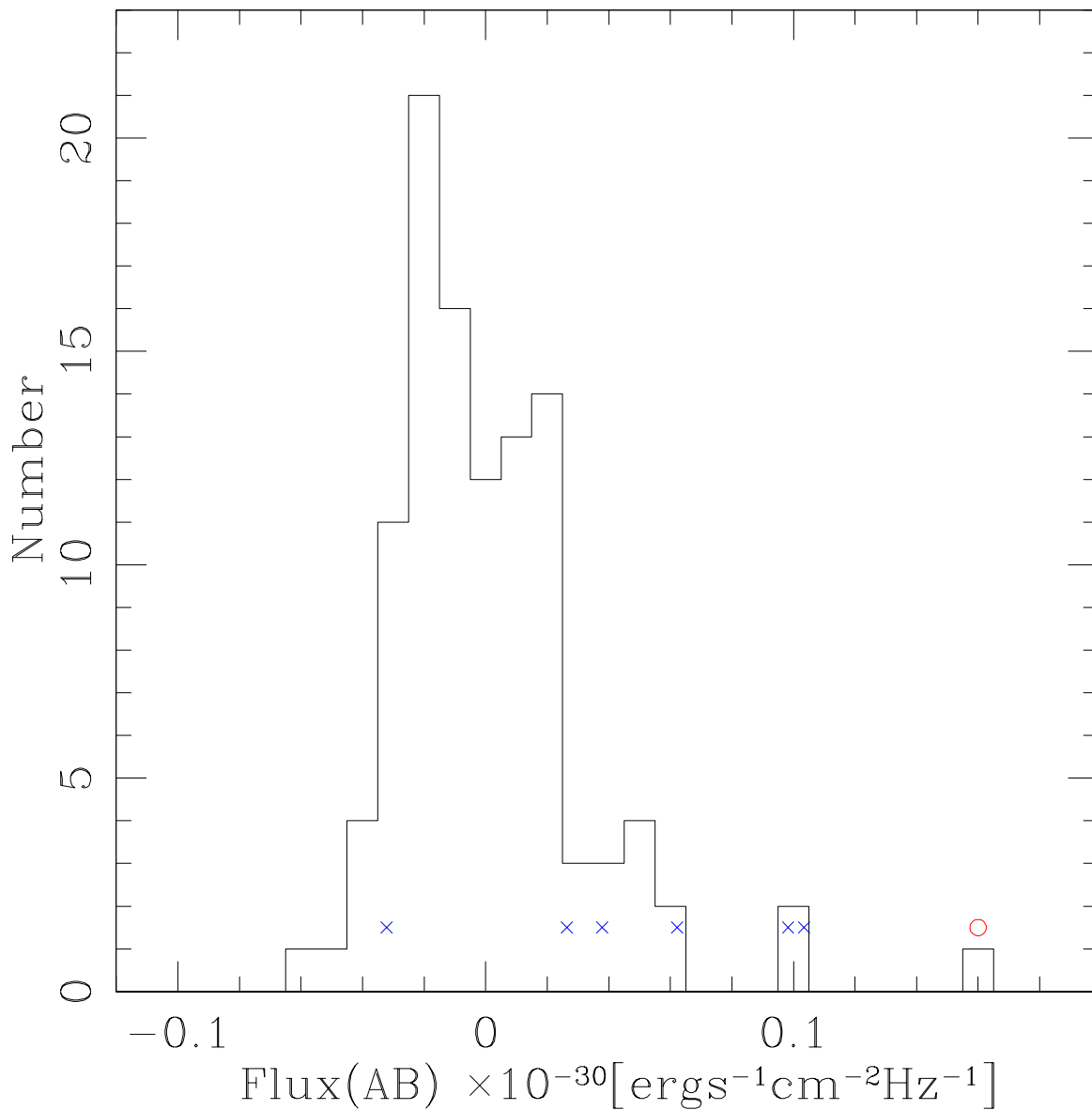


Fig. 9.— Flux distribution of the clean LBG sample (102) and AGNs (6) in AB units and within $1.2''$ diameter aperture is shown. AGNs are marked with blue crosses, and the LBG with a red circle. Three AGNs (from right to left) and the LBG (circle) have been detected in their LyC with S/N higher than 2 (see also Table 3).

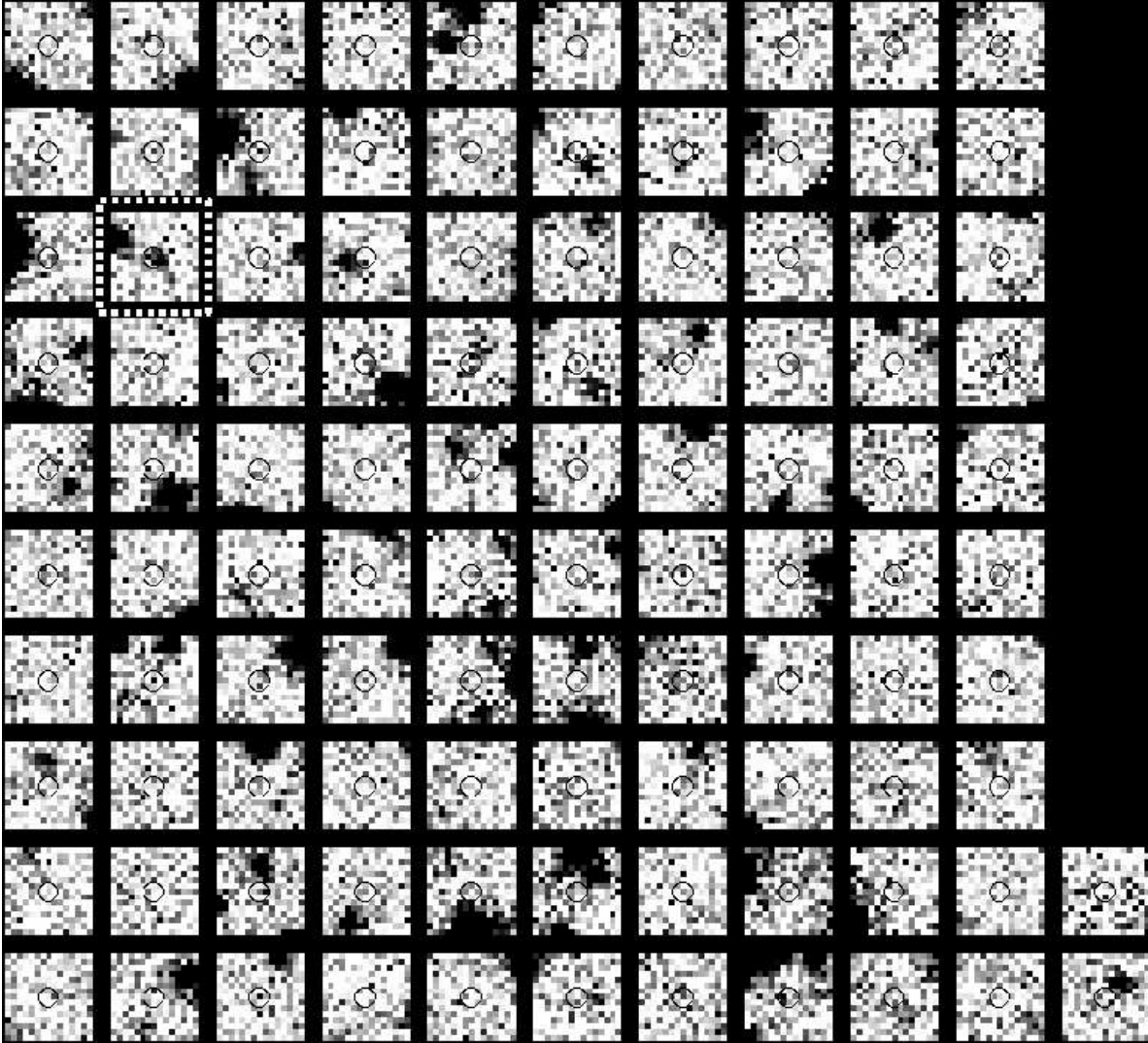


Fig. 10.— VLT/VIMOS U -band cutouts of the sources adopted in the simulations (clean sample). The box sizes are $4.5''$ on a side. The sole LBG detected in LyC with S/N higher than 2 in the $1.2''$ diameter aperture is marked with a dotted square (GDS J033216.64-274253.3 with S/N=5.5, described in Sect. 3.2.1). Circles indicate the position of the $1.2''$ diameter apertures.

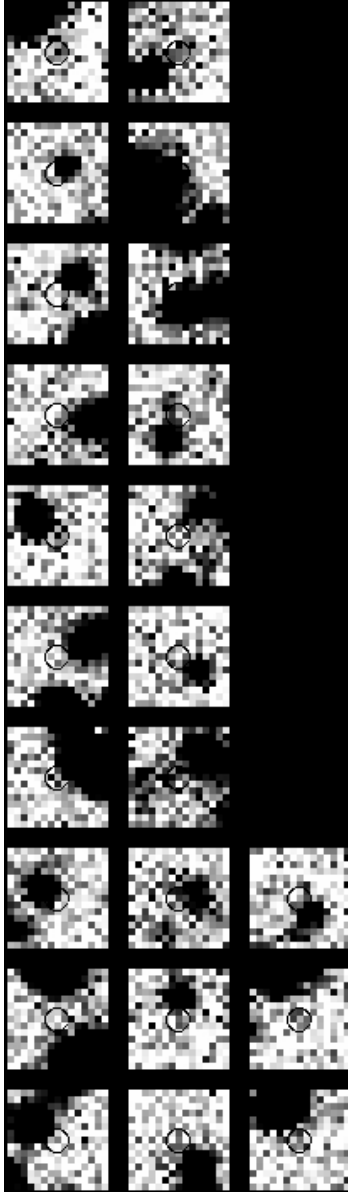


Fig. 11.— VLT/VIMOS U -band cutouts of the sources excluded from the simulations because of the presence of a nearby blue object. The box sizes are $4.5''$ on a side (see text for details).

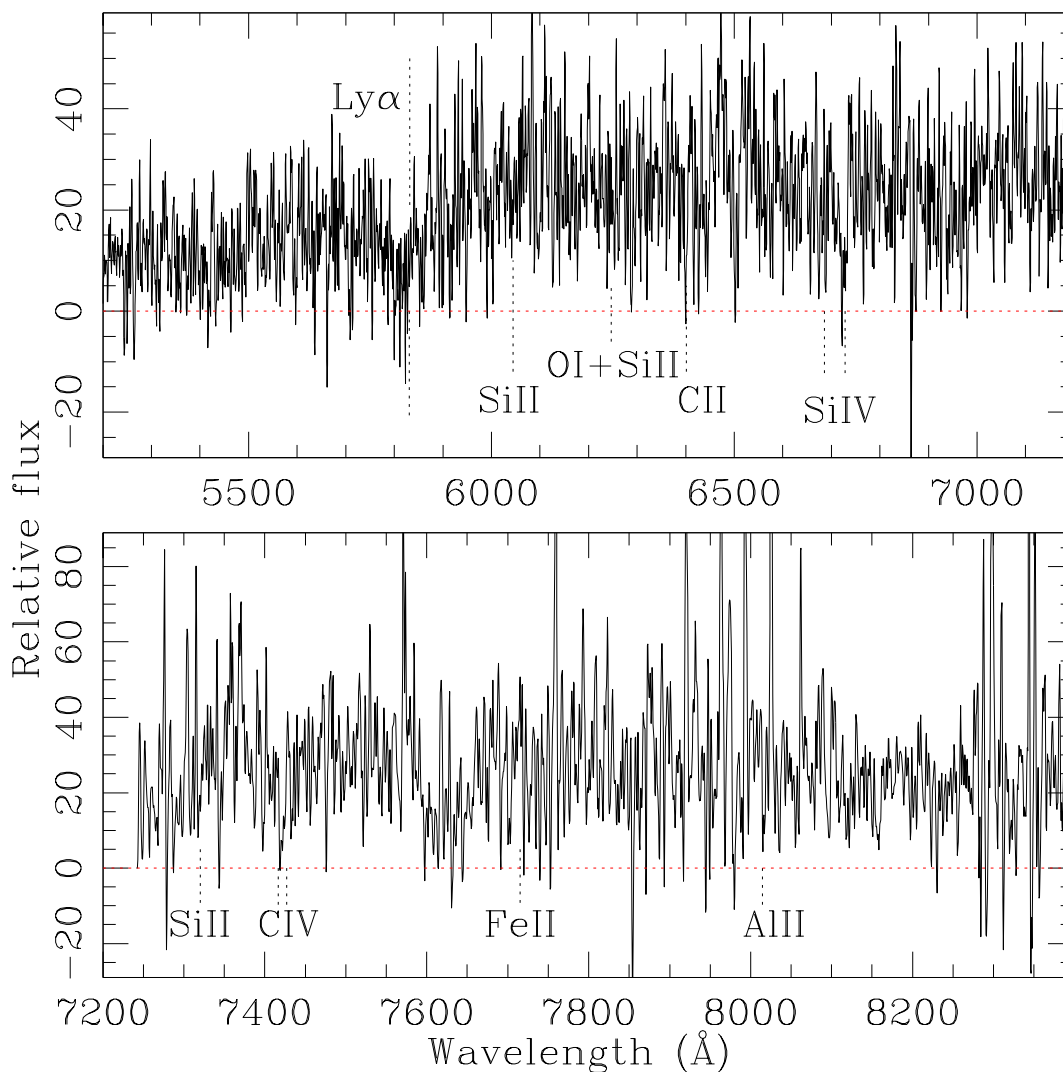


Fig. 12.— Extracted Keck-DEIMOS spectrum of the LBG GDS J033216.64-274253.3 with LyC detection in the IB image ($S/N \simeq 5.5$). In the top and bottom panels the blue and red parts of the spectrum are shown; Ly α , SiIV 1403Å and CIV 1548-1550Å absorptions are clearly seen, and we marginally detect CII 1335Å absorption. Absorption from SiII 1260, OI+SiII 1302-1304, SiII 1526, FeII 1608 and AlIII 1671 are not detected, nor are emission lines like NiV] 1486 and HeII 1640 detected. A comparison with the cB58 spectrum with the IRAF task *rvsao* gives a good cross correlation coefficient ($R=3.34$) and a redshift of 3.797.

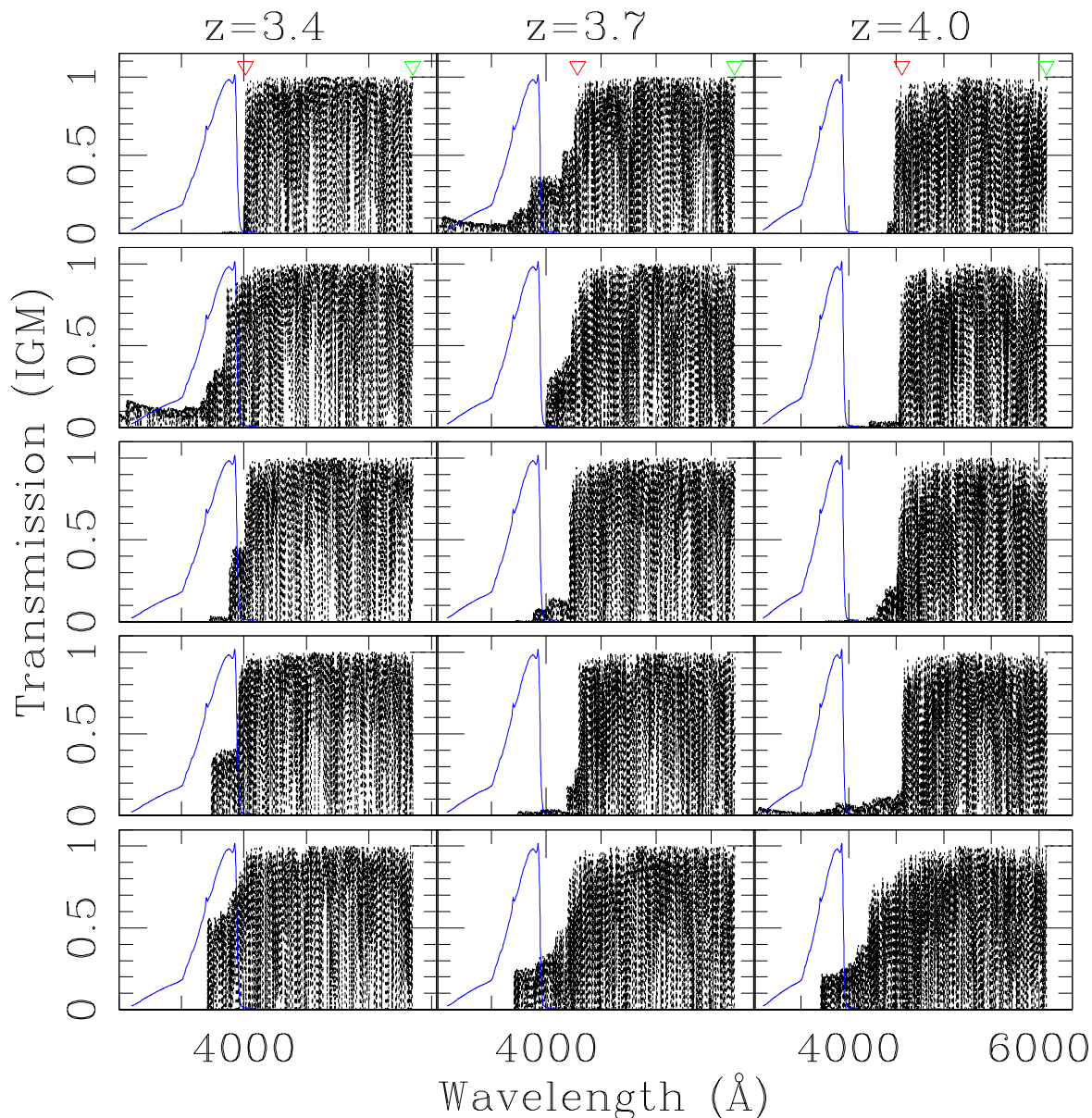


Fig. 13.— Examples of IGM transmission derived from the IW08 models for three redshift values. Zero transmission at blue wavelengths occurs when there is a LLS or DLA system at lower redshift. The IB filter shape is shown as dotted blue lines and in the top panels the positions of the 912\AA Lyman limit and Ly α are marked with open red (left) and green (right) triangles, respectively.

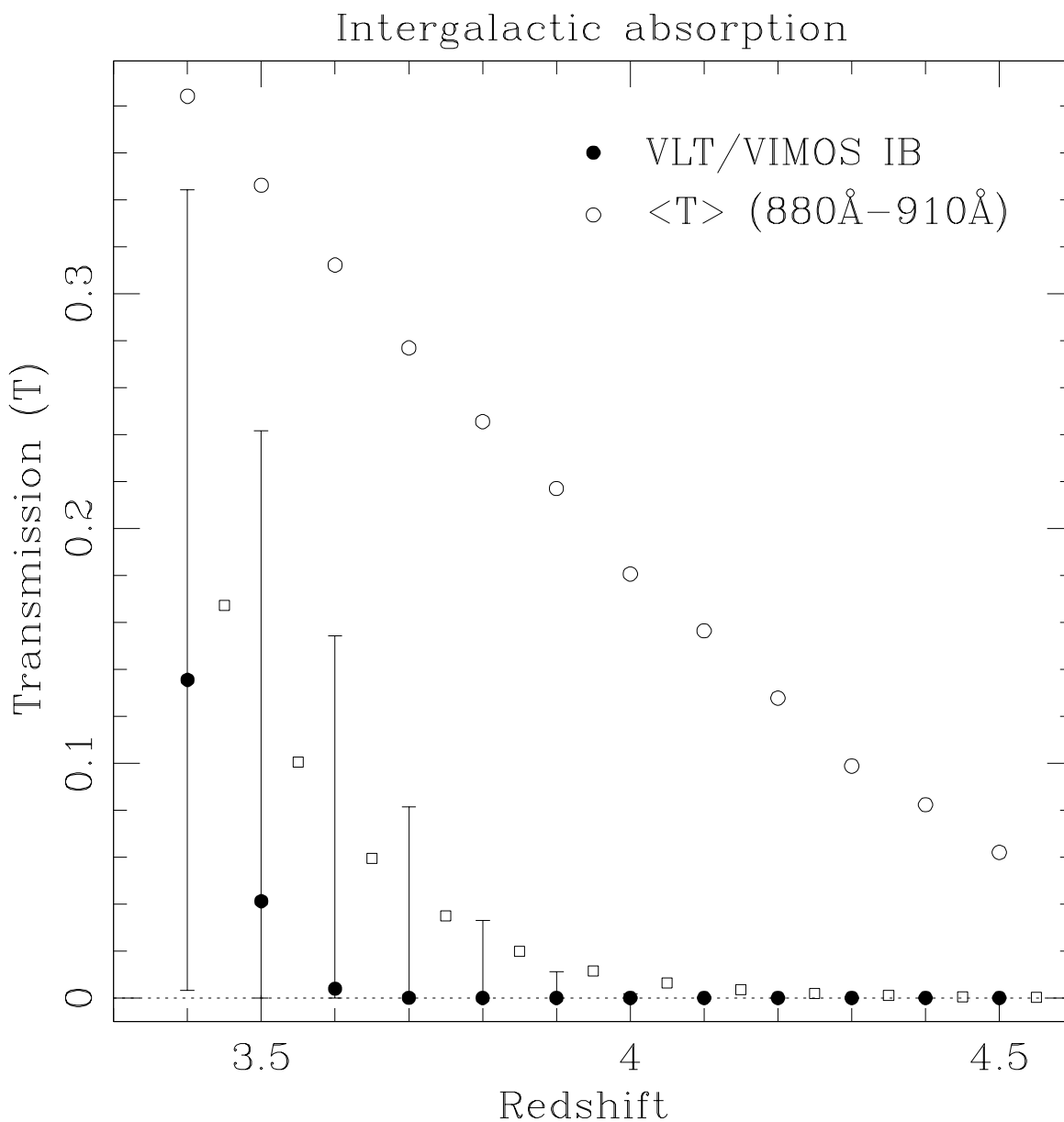


Fig. 14.— Transmission averaged over the wavelength range of the LyC (880-910 Å) (open circles) and convolved with the VLT/VIMOS IB filter (filled circles) as a function of source redshift. The filled circles and vertical error bars indicate the median value and central 68% range of the transmission for the 10,000 lines of sight generated with the IW08 simulations. Open squares are the averages calculated over the same lines of sight (shifted by $dz=0.05$ to the right for clarity). Clearly the VLT/VIMOS IB probes progressively shorter wavelengths as redshift increases, with the effect of lowering the transmission.

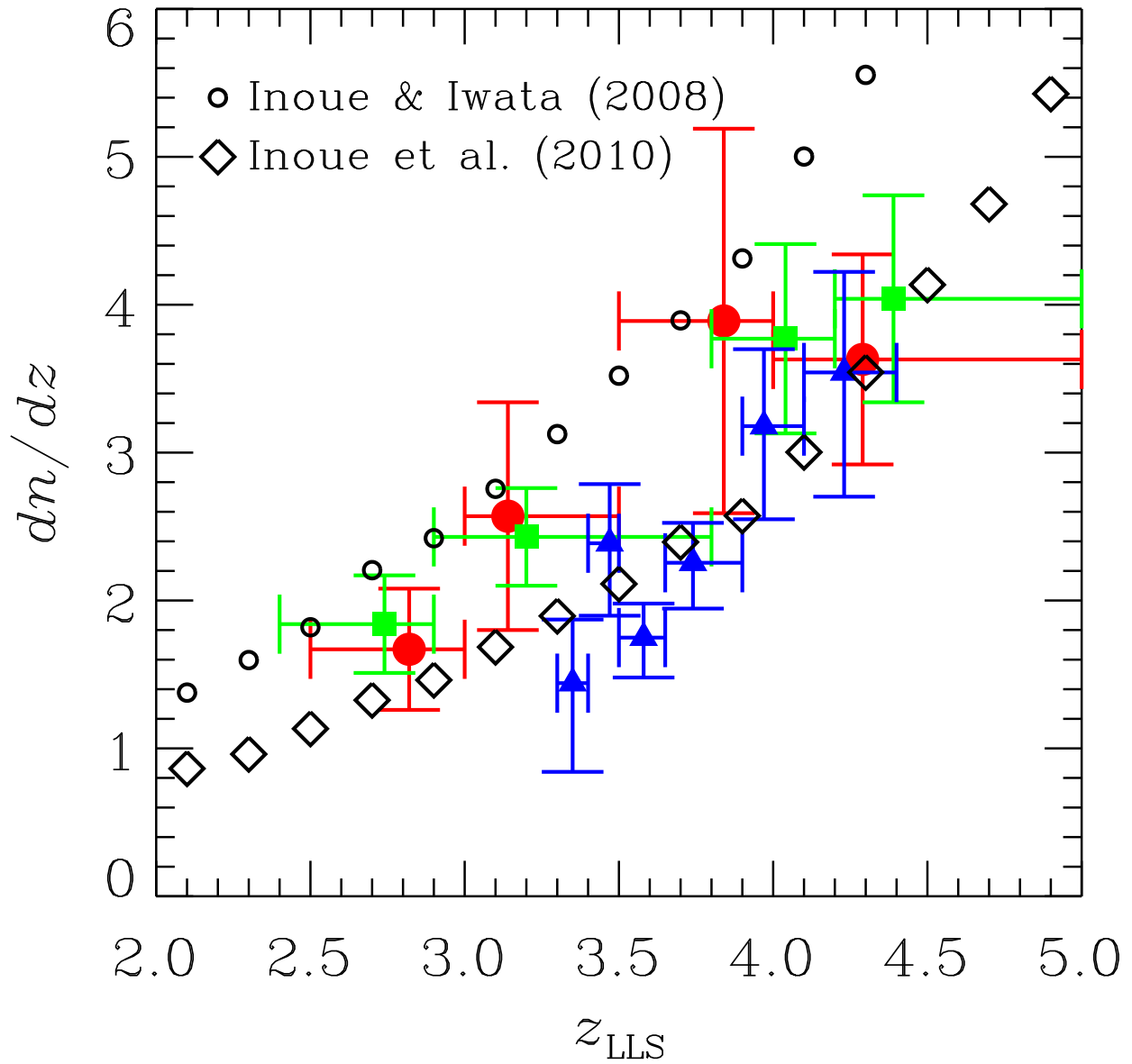


Fig. 15.— Number density of LLSs vs. redshift reported from previous and recent works. The filled circles are estimations of Péroux et al. (2005), squares are Songaila & Cowie (2010), and triangles are Prochaska et al. (2010). Open circles are the number density adopted in IW08, while diamonds are that assumed in the updated simulation by Inoue et al. (2010).

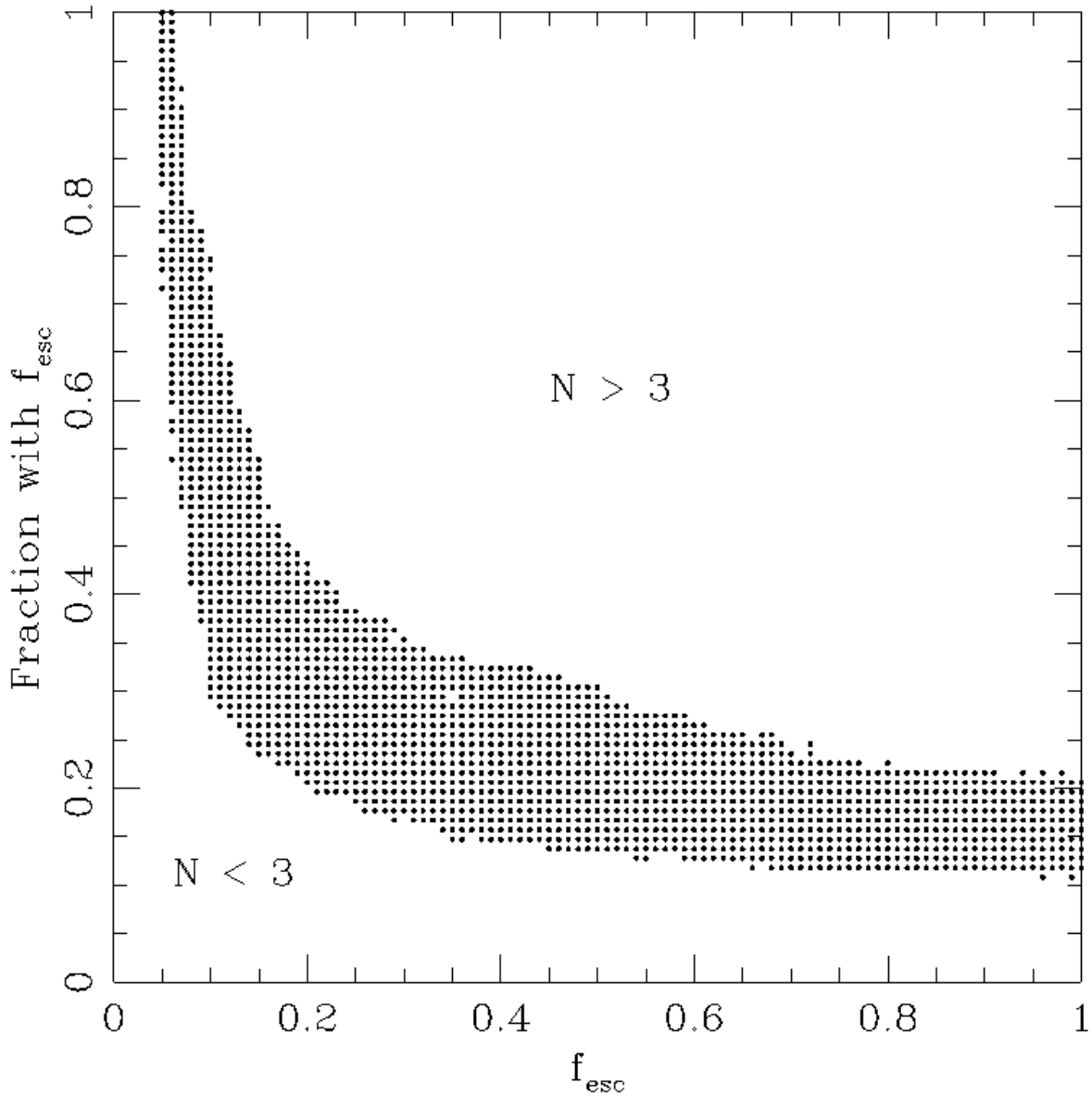


Fig. 16.— Parameter space excluded by a Monte Carlo analysis described in the text. The x-axis is the escape fraction (f_{esc}), and the y-axis is the fraction of galaxies that have this escape fraction. The other galaxies are assumed to have negligible escape fractions. The shaded region correspond to a number of expected LyC detections in the IB survey equal to 3. The fact that only 1 out of 102 LBGs has been detected suggest that our observations are compatible with the region where $N < 3$, implying that large fractions of the sample with high f_{esc} are excluded ($N > 3$).

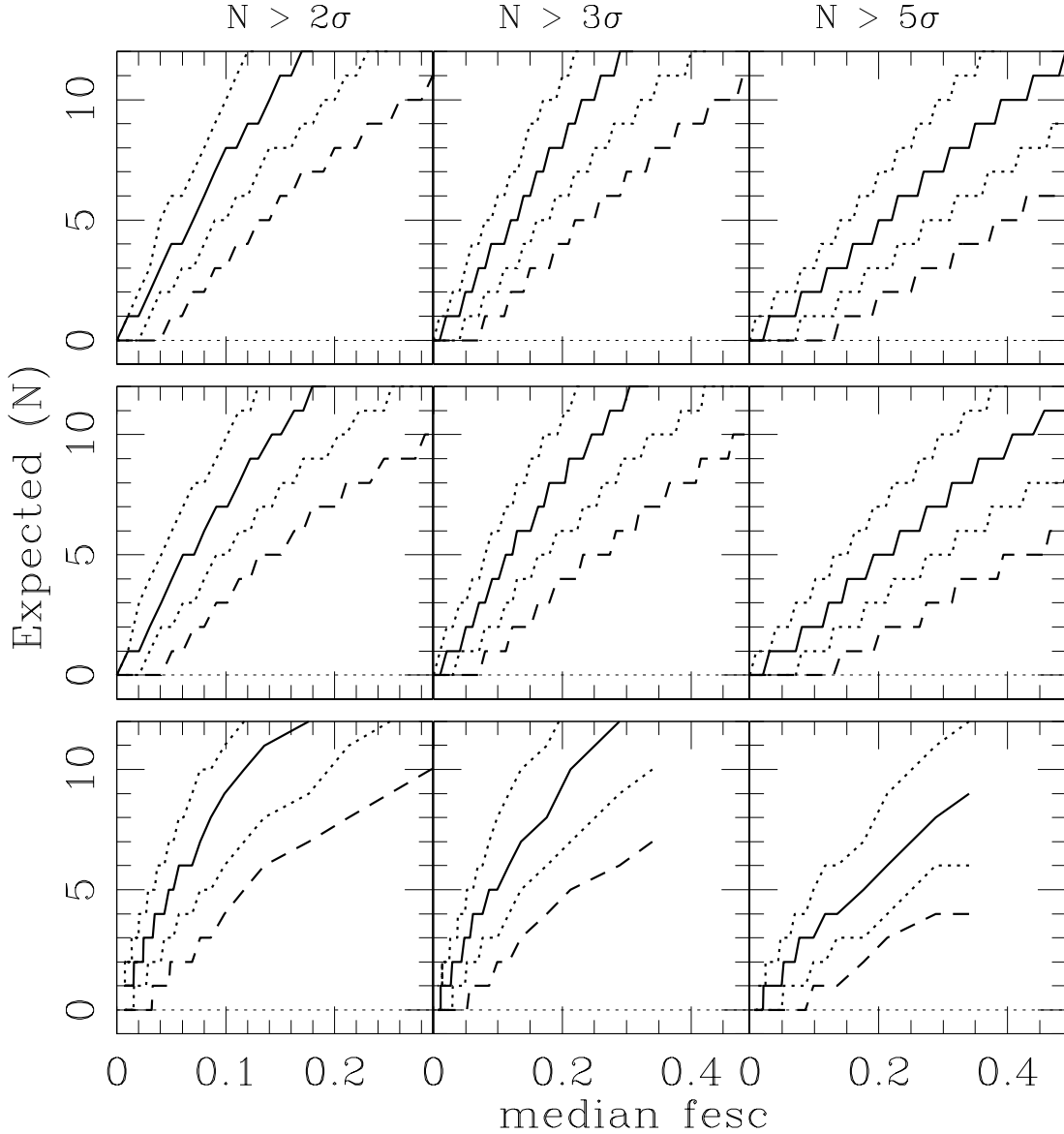


Fig. 17.— Monte Carlo simulations of the expected number of LyC detections in the ultra-deep VLT/VIMOS U -band imaging as a function of the median f_{esc} (in the left panels f_{esc} up to 30% is shown, in the middle and right panels it is shown up to 50%). From left to right, the expected number of LyC detections are presented for three IB depths, 2σ (29.5), 3σ (29.1) and 5σ (28.6), respectively. Solid lines show the median expected number, while the dotted lines and dashed line mark the one sigma and three sigma limits, respectively. In the top panels a constant f_{esc} value is assumed, from 1% to 100%. In the middle and bottom panels Gaussian and exponential distributions of f_{esc} with different medians are shown, respectively. The abscissa reports the median of the simulated distribution (see text for details).

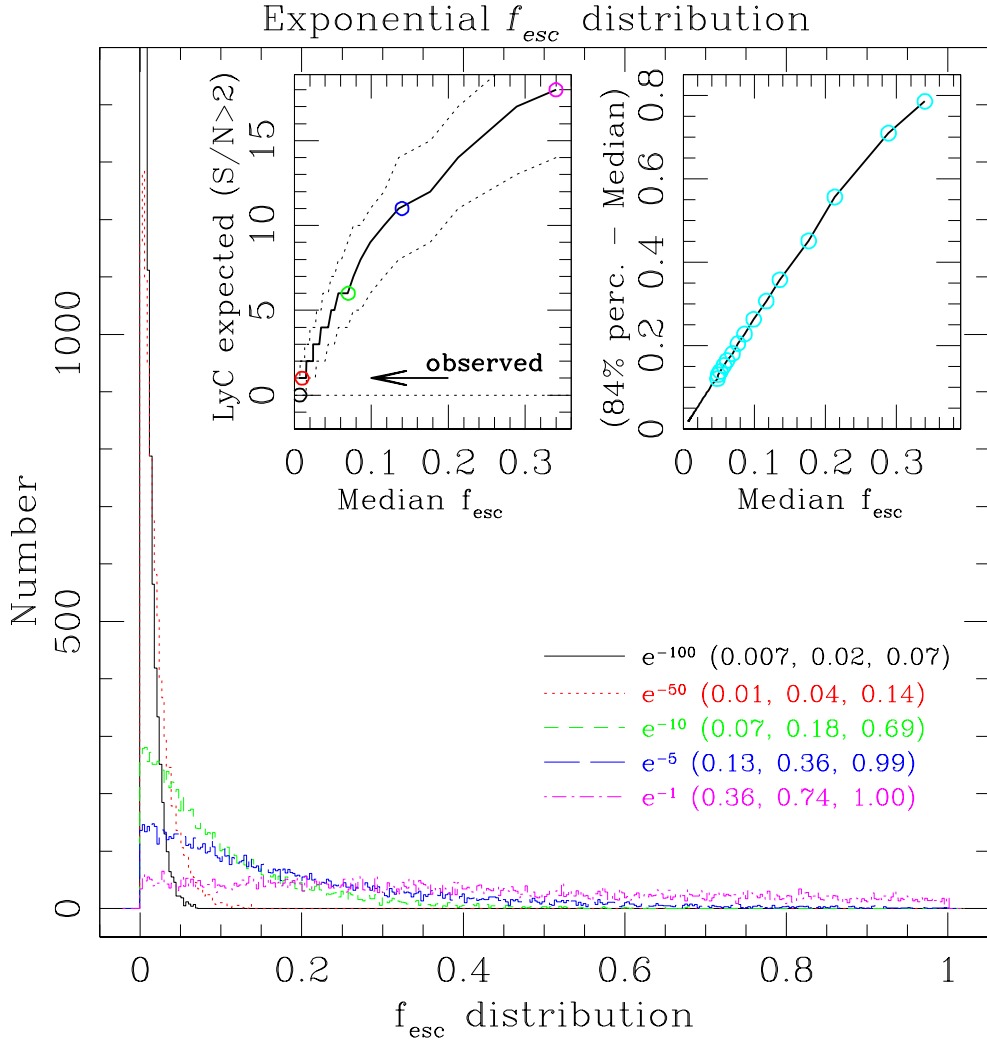


Fig. 18.— **Left inner box:** Monte Carlo simulations of the expected median number of LyC detections in the ultra-deep VLT/VIMOS U -band imaging (thick solid line) and 68 percent central interval (dotted lines) reported as a function of the median of the 100 exponential distributions explored (different slopes λ have been explored). Color-coded open circles correspond to the examples of distributions shown in the main box. **Right inner box:** The black solid line outlines the region occupied by the 100 distributions in the plane (1σ , median). The distributions for which the expected number of LyC detection is larger or equal to 5 (probability less than 5% to observe ≤ 1 LyC detection) are shown with open cyan circles. **Main box:** Examples of exponential distributions of f_{esc} with $\lambda=1, 5, 10, 50, 100$ are shown (10,000 extractions for each one have been done). The numbers reported in the legend from left to right are the median, the 84% percentile and the maximum value, respectively.

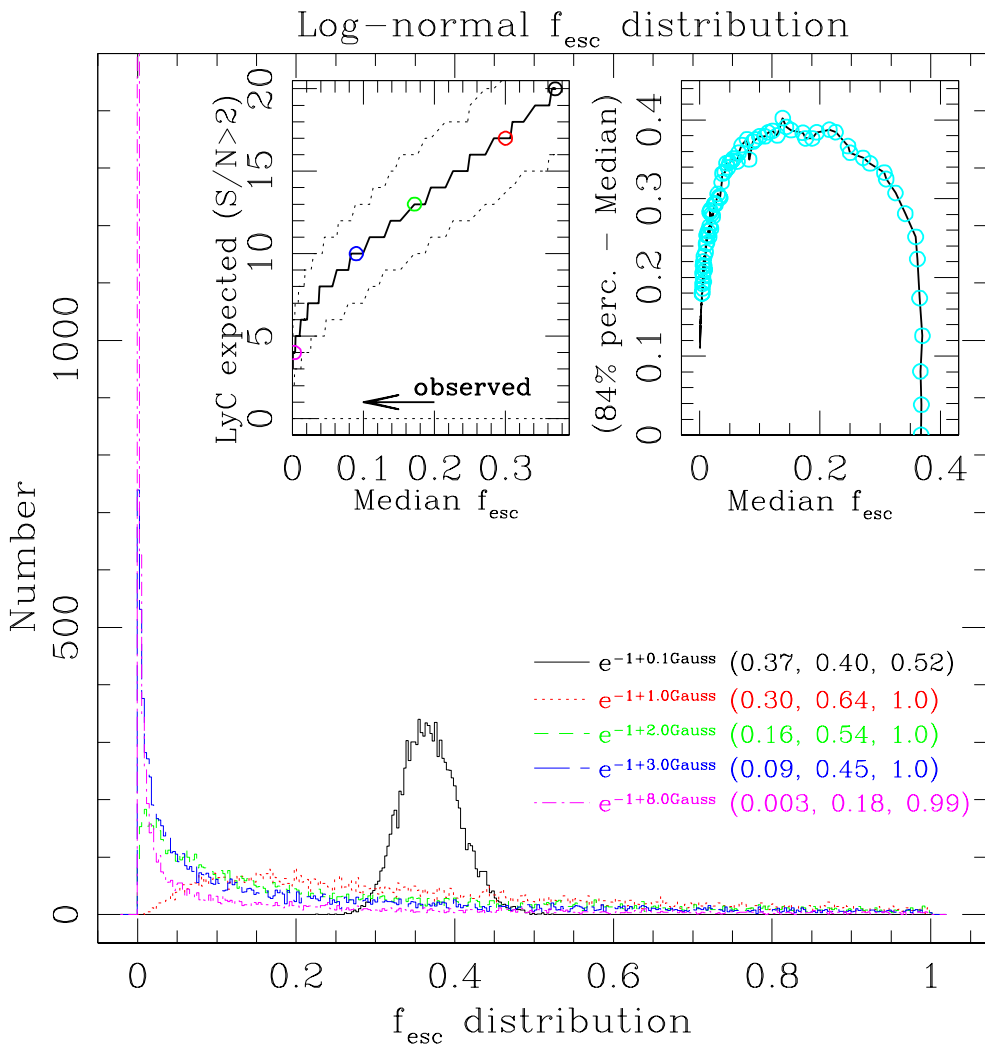


Fig. 19.— **Left inner box:** Monte Carlo simulations of the expected median number of LyC detections in the ultra-deep VLT/VIMOS U -band imaging (thick solid line) and 68 percent central interval (dotted lines) reported as a function of the median of the 100 log-normal distributions explored (the case with $K=1$ and λ running from 0.1 to 10 with step 0.1 is shown). Color-coded open circles correspond to the examples of distributions shown in the main box. **Right inner box:** The black solid line outlines the region occupied by the 100 distributions in the plane (1σ , median). The distributions for which the expected number of LyC detection is larger or equal to 5 (probability less than 5% to observe ≤ 1 LyC detection) are shown with open cyan circles. **Main box:** Examples of log-normal distributions of f_{esc} with $\lambda=0.1, 1.0, 2.0, 3.0$ and 8.0 are shown (10,000 extractions for each one have been done). The numbers reported in the legend from left to right are the median, the 84% percentile and the maximum value, respectively.

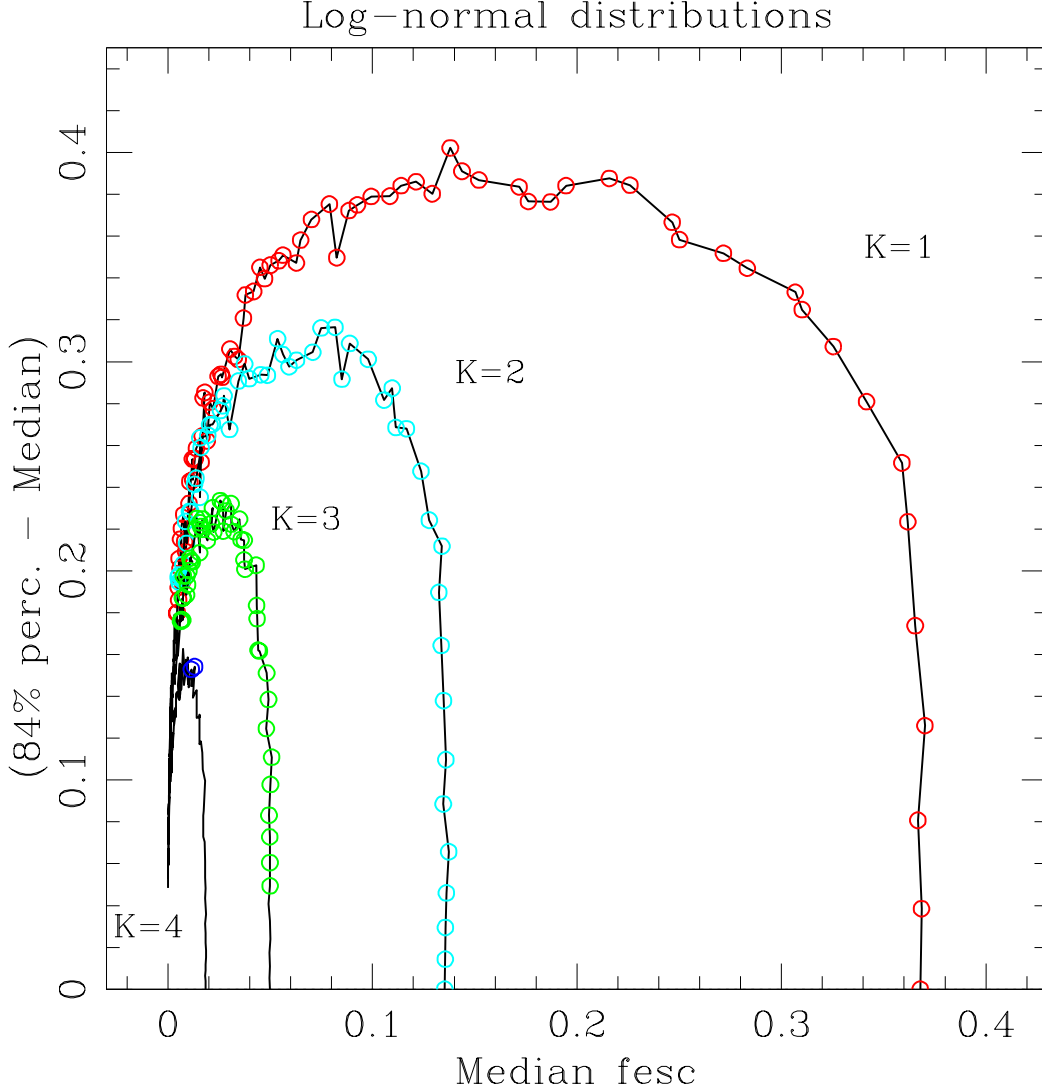


Fig. 20.— The same as shown in the inner right box of Figure 19, but calculated for different K values of the log-normal distributions ($e^{-K+\lambda \times Gauss}$). The black solid lines show the regions occupied by the 100 distributions for each K value. The distributions for which the expected number of LyC detection is larger or equal to 5 are shown with open circles. The single observed LyC detection reported in the present work suggests that f_{esc} is distributed with median and 1σ upper tail lower than $\sim 6\%$ and 18% , respectively, if a log-normal distribution is assumed.

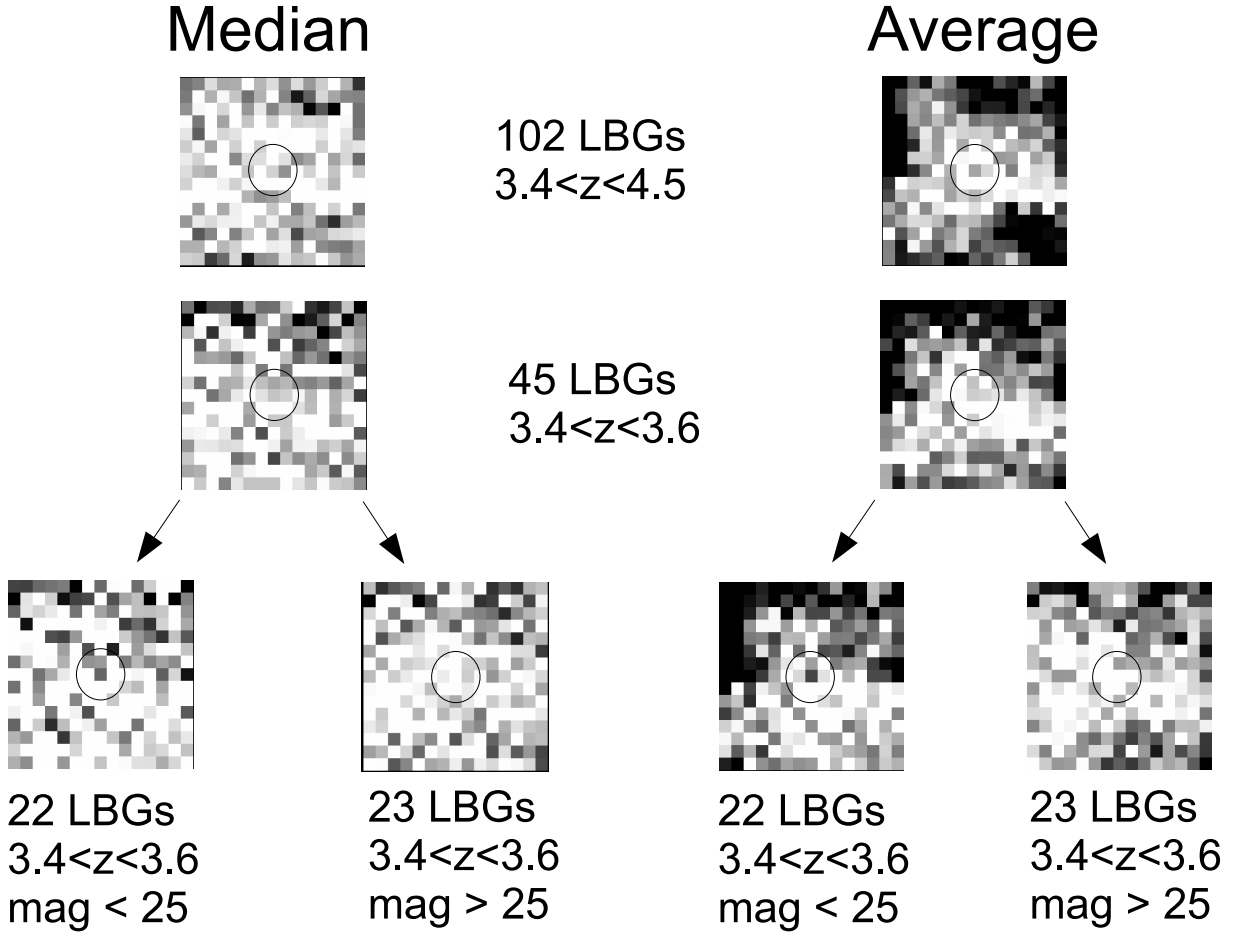


Fig. 21.— Median stacking of LBGs from the *clean* spectroscopic sample. Stacking of redshift-selected sub-samples has been performed in order to increase the IGM transmission, as well as for the brighter ($i_{775} < 25$) and fainter ($i_{775} > 25$) sub-samples (see text). The pixel size is $0.3''$ and each box is $4.5''$ on a side. The circles have diameters of $1.2''$.

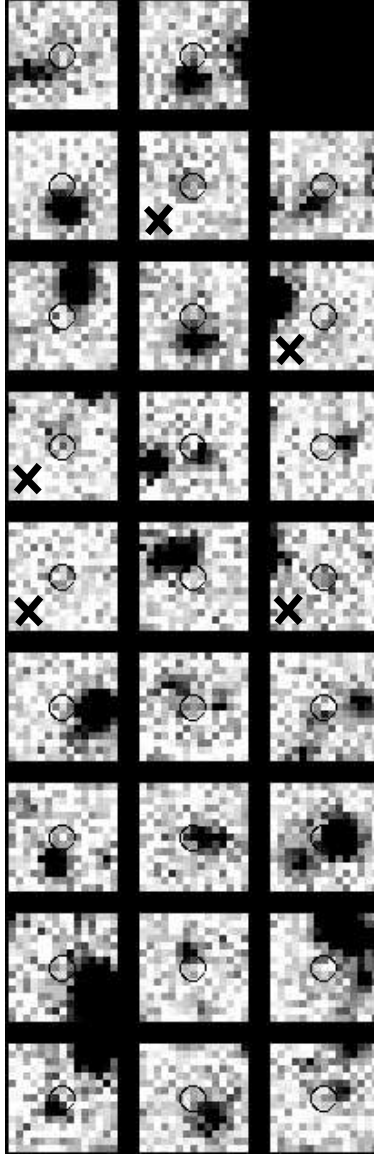


Fig. 22.— VLT/VIMOS U -band cutouts of the sources selected in the HUDF with magnitude $27 < i_{775} < 28.5$, photometric redshifts in the range $3.4 < z_{\text{phot}} < 4.0$ and S/N ratio in the $1.2''$ diameter aperture higher than 2. The size of the boxes is $4.5''$ on a side. Sources indicated with a black cross show a non-offset detection in the IB.

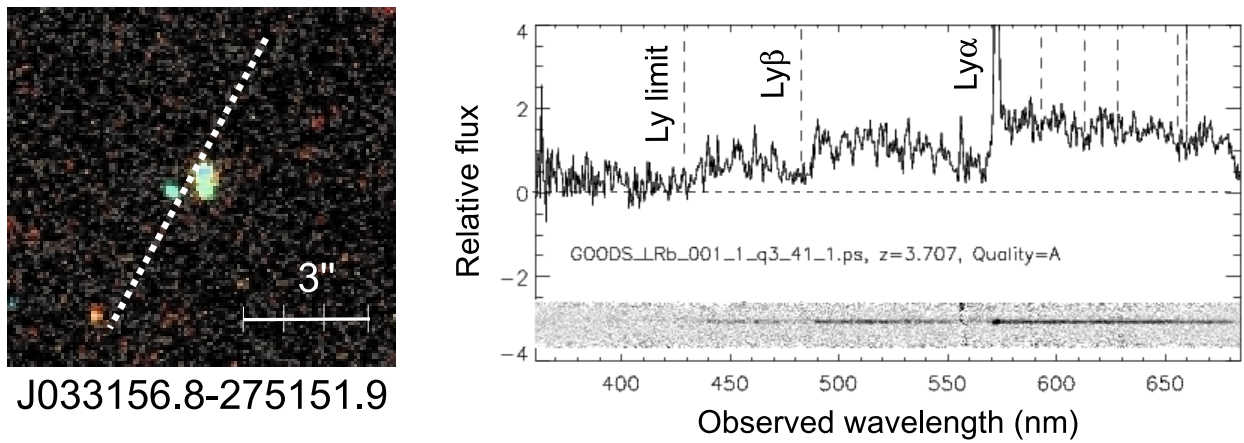


Fig. 23.— Two-dimensional spectrum of the source GDS 033156.8-275151.9 in the outer region of the GOODS-South. On the left side the *HST*/ACS color image derived from the GEMS survey; the dotted line shows the slit orientation in the sky. As discussed in the text, a compact source close to the LBG (center) at sub-arcsecond separation is clearly visible (to the left). The spectrum (right part of the figure) contains the contribution of both sources. In particular, faint flux is detected below the Lyman limit, most probably due to the close (lower redshift) companion.